AD-A146 549 ANISOTROPY AND MICROSTRUCTURE OF RARE EARTH PERMANENT MAGNET MATERIALS. (U) TECHNISCHE UNIV VIENNA (AUSTRIA) INST OF APPLIED AND TECHNICA.. J FIDLER ET AL. JUN 84 1/1

UNCLASSIFIED R/D-4060-R-MS DAJA45-84-C-0010 F/G 20/3 NL

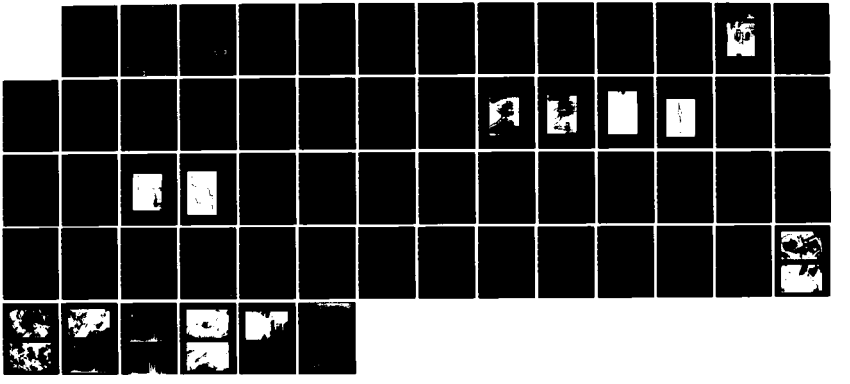

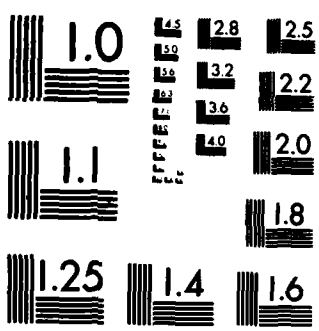

ANISOTROPY AND MICROSTRUCTURE OF RARE EARTH PERMANENT MAGNET MATERIALS

by

Josef Fidler
Roland Grössinger
Hans Kirchmayr
Peter Skalicky

1ST SEMI-ANNUAL REPORT: Jan. 1984 - June 1984

CONTRACT NO.: DAJA 45-84-C-0010

Peter Skalicky
Institute of Applied and Technical Physics,
Technical University of Vienna,
Karlsplatz 13, A-1040 Vienna, Austria

"The Research reported in this document has been made possible through the support and sponsorship of the U.S. Government through its European Research Office of the U.S. Army. This report is intended only for the internal management use of the Contractor and the U.S. Government."

The present contract concerns two different experimental projects:

A) MAGNETIC ANISOTROPY INVESTIGATIONS

B) THE STUDY OF THE MICROSTRUCTURE OF PERMANENT MAGNETS BY MEANS OF ELECTRON MICROSCOPY

A) MAGNETIC ANISOTROPY INVESTIGATIONS

by

G. Grössinger, P. Obitsch and
H. Kirchmayr
Institute of Experimental Physics
Technical University of Vienna
Karlsplatz 13,
A-1040 Vienna, Austria.

Content

1) Introduction

2) Experimental progress

3) Nd-Fe-B-magnets
   3.1) Magnet production
   3.2) Anisotropy measurements
   3.3) Hysteresis measurements
   3.4) AC-Susceptibility
   3.5) Thermal expansion
   3.6) Conclusion

4) Proposed developments
   4.1) Technical improvements
   4.2) Scientific proposal

1) Introduction

RE-Co magnets are well known as the materials which can be used for high level applications. Physically two basic componends are of importance:

i) $SmCo_5$ which has a saturation moment of $4\pi M_s \sim 11,2$ kg

ii) Sm_2Co_{17} with a value for $4\pi M_s$ 12,8 kg

Necessary demands for a material usable as a permanent magnet, are beside a high Curie temperature T_c, high values for the saturation magnetization and for the coercivity H_c. Whereas T_c and M_s are intrinsic properties, H_c depends on the metallurgical process. However a large coercivity is only possible, if the anisotropy is high enough. The anisotropy field H_a is generally a theoretical limit for H_c. For some magnets the shape anisotropy must be taken into account, but for the materials of interest in this work, this type of anisotropy is neglected. The coercivity mechanism of a $SmCo_5$ magnet is principally different to that of a Sm_2Co_{17} magnet. The former material is grinded to nearly monodomainic particles. The existence of reverse domains causes, compared with the theoretical limits, a distinct lower value of H_c which is of the order of 20 kOe. Contrary to $SmCo_5$ are the hard magnetic properties of a Sm_2Co_{17} magnet based on the existence of precipitates where the domain walls are pinned. The complicated microstructure as studied with an electron microscop was discussed in (1).

For technical applications the following main differences exist:

i) $SmCo_5$: $(BH)_{max} \sim 20$ MGOe, $_IH_c \sim 20$ kOe
$4\pi M_s \sim 11,2$ kG, $T_c = 1020$ K, $H_a \sim 350$ kOe

ii) Sm_2Co17: $(BH)_{max}$ 30 MGOe, $_IH_c$ 10 - 15 kOe
$4\ M_s$ 12,8 kG, $T_c = 1195$ K, $H_a \sim 70$ - 100 kOe

This means that Sm_2Co_{17}-magnets exhibit the higher energy product, however generally a lower coercivity. The stability against corrosion is due to the larger particle size better

for 2/17 magnets. The main disadvantages of all RE-Co magnets are the high costs of the raw material. Recently a new family of hard magentic materials based on Nd-Fe-B was developed (2,3). With these compounds permanent magnets with energy products up to 40 MGOe were produced (4). The greater abundance of Nd combined with the low price for Fe are a hope for producing high qualitativ, low cost magnets in the future. Therefore large scale applications are proposed for Nd-Fe-B magnets. The aim of the scientific part of the present report will be the investigation of the low temperature physical properties of these new family of compounds.

Due to the large values of the anisotropy fields as well as of H_c, high field measurements are necessary in order to study these materials. Table I compares the possibilities of different field generating methods.

Table I: Field generation

Field-Device	H_{max} (kOe)	possible accuracy	Advantage	Disadvantage
Fe-Yoke	20 - 30	good	works at RT inexpensive closed magn. circuit N=Ø	low field
Supercond. coil	up to 150	good	liquid He necessary	expensive, open magnet circuit N≠Ø
Pulsed field	easy: 100-150 up to 500	good bad *)	works at RT inexpensive	open magnet circuit N≠Ø measuring troubles

RT ... room temperature
N ... demagnetizating factor

*) The measuring problems in pulsed fields are up to now not commercially solved. Hysteresis measurements with an accu-

racy of 1% seems to be possible, if besides electronically solvable problems, calibration standards with the corresponding accuracy are available. This subject was discussed in more ditail by (5). In the last report the set up of our pulsed system ($H_{max} \sim 260$ kOe), which works between 4,2 K and 300 K was described (1). The technical part of the present work is focused on the development of a high temperature equipment which can be used in pulsed fields.

2) Experimental progress

Our pulsed field system consists of a 8mF condensator battery, which can be charged up to 2500 V (stored energy 25 kJ). The discharge through a copper magnet is performed by an ignitron. The pulse duration is 5 - 10 ms. The possibe pulse shapes are sin-half-wave, sin-full-wave and crowbar. The magnet is a fiverglass-reinforced magnet, the maximum field is between 250 - 280 kOe, with a homogeneity of 1% over 20 mm, the usable inner diameter is 18 mm. The magnet is generally cooled in liquid nitrogen in order to reduce the losses. A set up where the magnet is cooled with liquid He in order to reduce the necessary inner diameter was also constructed.

The system is generally used to measure the hysteresis loop M(H), the possible accuracy is 3 - 4 %. Studies comparing with static M(H) measurements showed, that the error is not caused by eddy currents. The main problems are resulting from calibration errors and digital errors (6). An improvement is expected using a transcient recorder with a higher sensitivity. A further important application is the measurement of the anisotropy field H_a using the SPD-technique (7). Especially the temperature dependence of H_a is a powerfull tool to get informations about local rearrangements, as was shown for Sm_2 (Co, Fe, Cu, Zr)$_{17}$ (8) and (Sm, Pr) Co_5 (9) magnets. Up to now only measurements between 4,2 K and room temperature are possible. This temperature range is scientifically interesting, e.g. in order

to test the One Ion model (10). However for technical applications the temperatures above RT are more interesting. Up to now only a few attempts were made to construct a high field, high temperature equipment (11,12).

2.1) High temperature set-up

The inner diameter of the magnet is 18 mm. The problem now is to construct a furnace, which is small enough to be positioned in the magnet. Additionally a pick-up system, a sample holder with a thermocouple must be arranged there. Naturally all used components should not disturb the measuring signal. Fig. 1 shows scematically the used set-up. The furnace was wound from a Pt-wire for a Al_2O_3-tube. Inside this tube a small sample can be positioned. The heated volume is therefore very small, less then 10 W are enough for the furnace. The temperature is measured with a Pt-PtRh thermocouple which is in close contact with the sample. A double quartz-tube isolates the hot zone from the pick-pu coil. A N/N pick-up system is outside, mechanically fixed on the high field magnet. All components inside the high field coil are not magnetic - except the sample. In order to avoid troibles from the heater current, a switching circuit interrupts the current during the high field shoot. Fig. 2 shows the electronic circuit for this application. Fig. 3 shows a photograph of the whole high field, high temperature equipment.

In order to test the apparatus, two kinds of measurements were made:

i) Measurement of the initial susceptibility $\chi_i(T)$ of pure Ni. This experiment is a test of the sensitivity and the correctures of the temperature measurement. Fig. 4 shows a block diagram of the used equipment. In this case a low AC-current flows through the pulse coil. The pick-up system detects a signal which is proportional to $(dM/dt)_{H\to\emptyset}$ $(\frac{dM}{dH})_{H\to\emptyset} = \chi_i(T)$. Approaching the Curie temperature T_C the magnitude X_i should decrease drastically. Fig. 5 shows the obtained $X_i(T)$ curve for Ni. the obtained T_C=353,8°C agrees

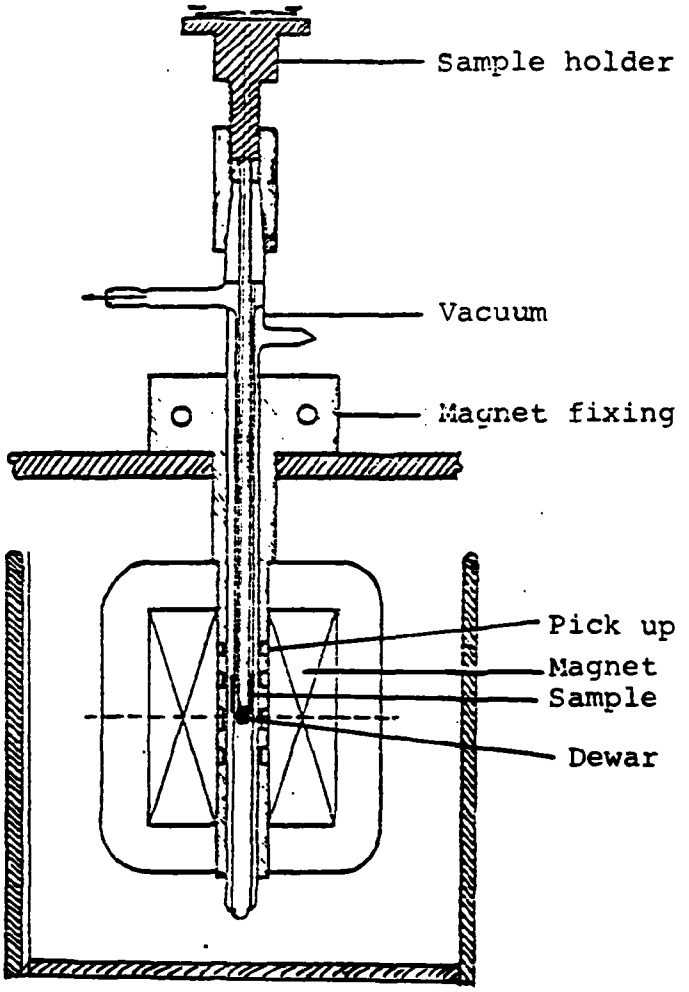

Fig.1: Scheme of the high temperature set-up

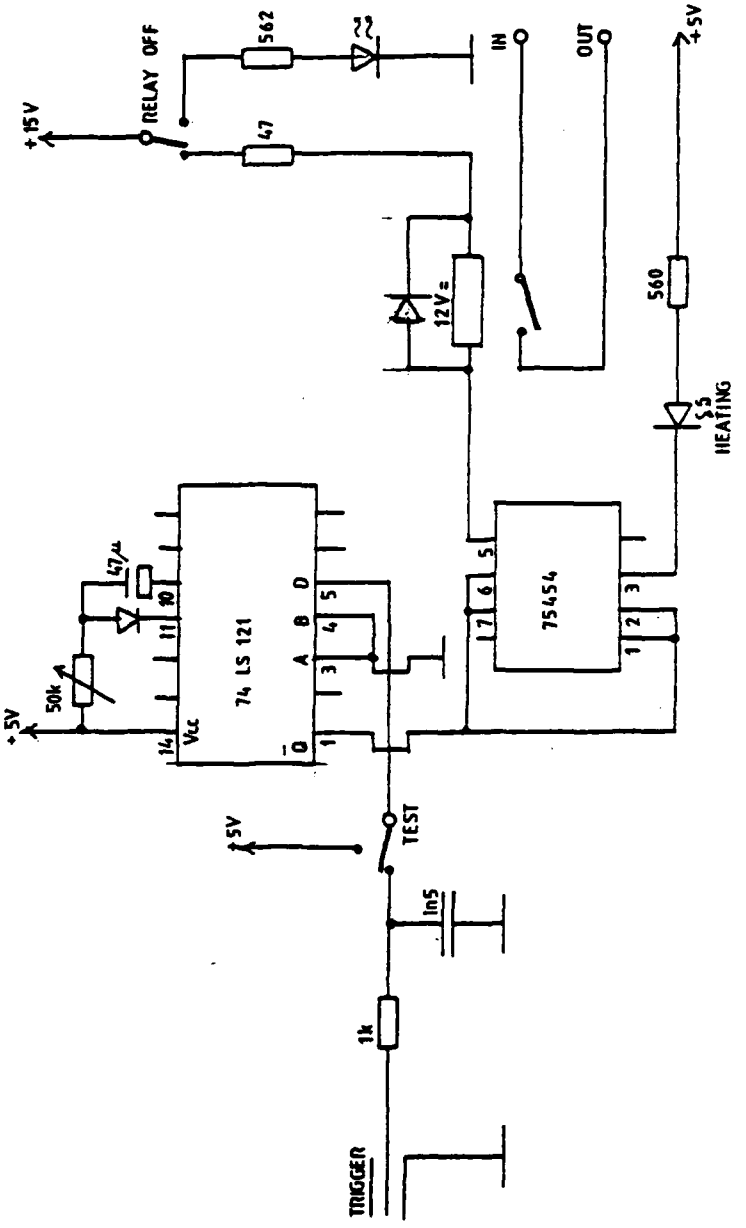

Fig.2: Electronic circuit of the heater control

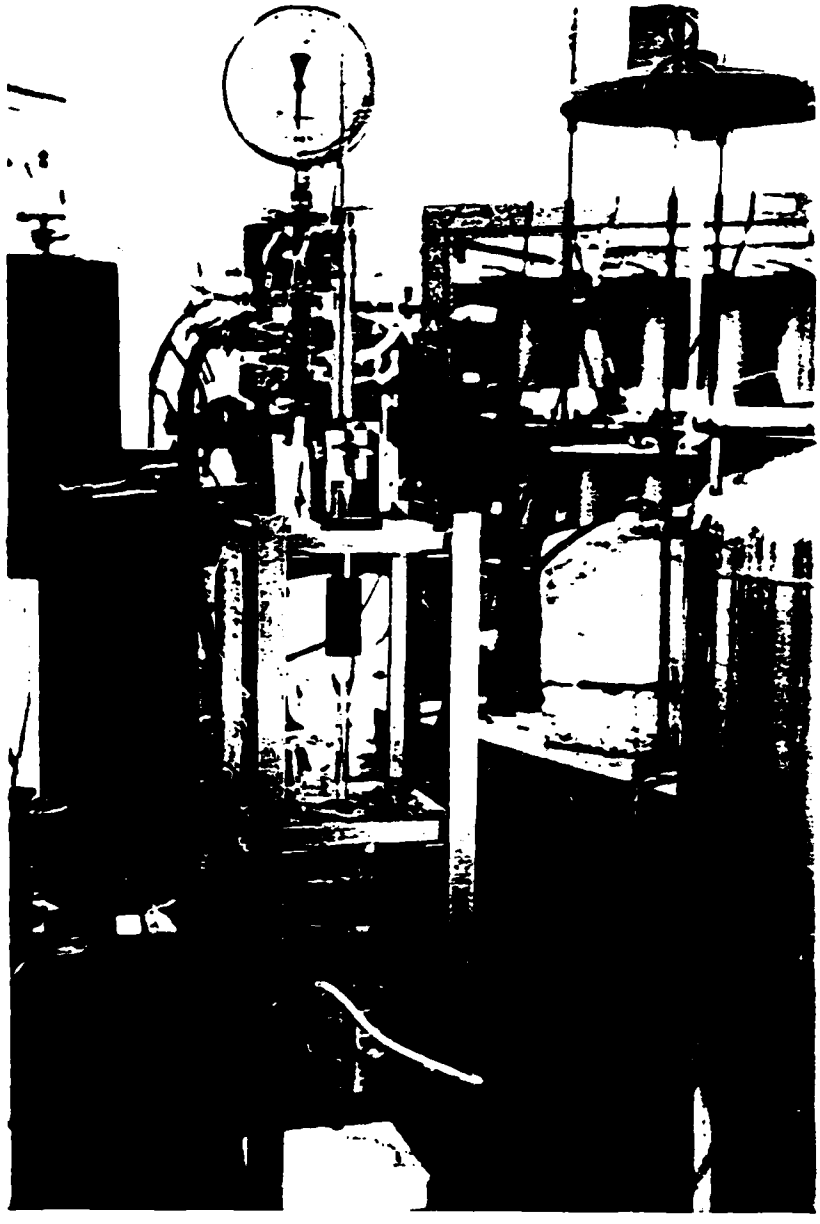

Fig.3: Photograph of the high temperature pulsed field equipment

Fig.4: Block-diagram for measuring the initial susceptibility

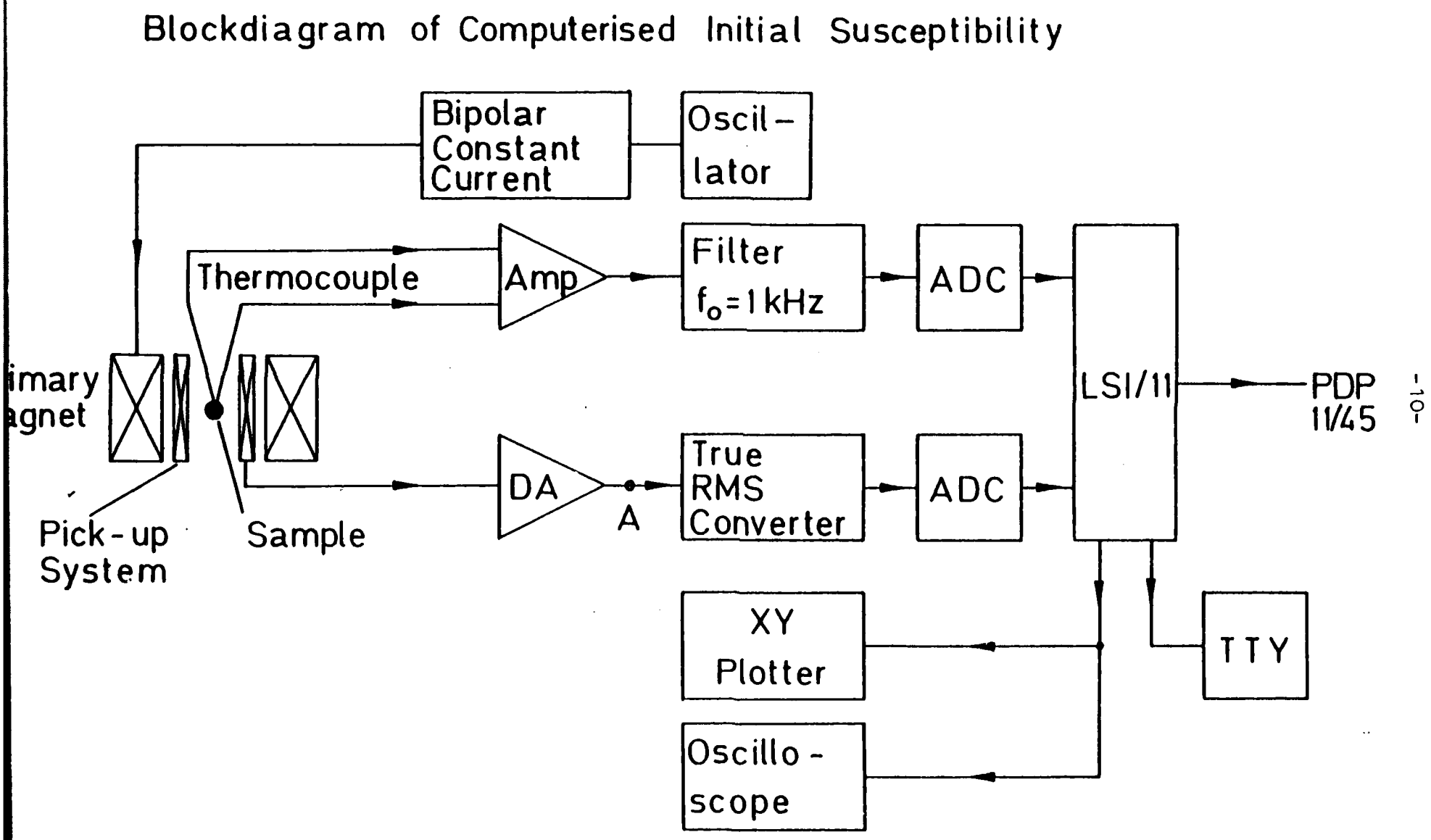

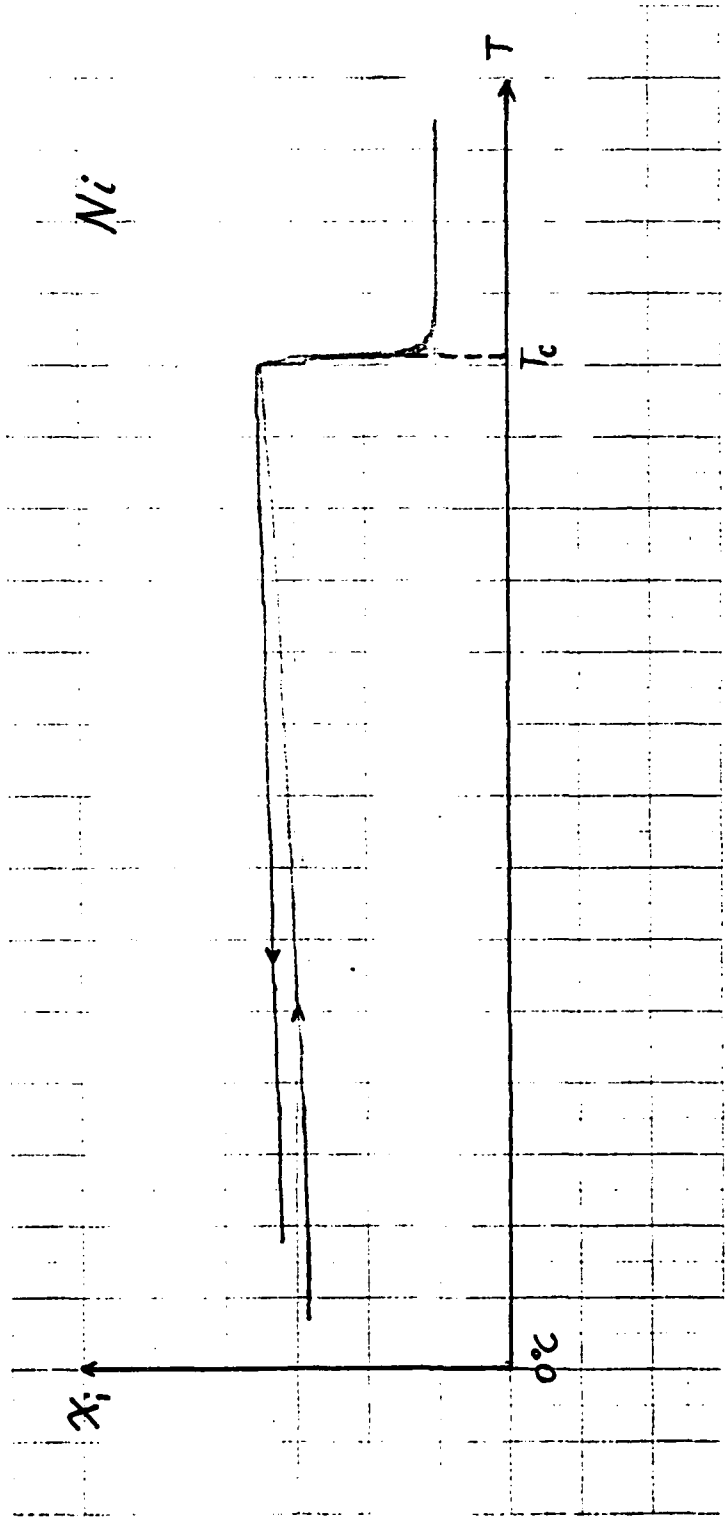

Fig.5: $\chi_1(T)$ measured for polycrystalline Ni
The measured value for T_c is 355,2°C

with the literature very well (13).
ii) Measurement of H_a (T) of Ba Fe_{12} O_{19} for T > RT using the SPD-technique. Fig. 6 composes H_a(T) as measured for polycrystalline Ba Fe_{12} O_{19} with single crystal data from (14). This demonstrates that the high temperature system works reasonable. Attempts to measure H_a for materials with higher anisotropy values where not successfull, because of a, with the field, dramatically increasing noise. The problem is due to the fact that the diameter of the sample is small compared to the diameter of the pick-up system. Additionally a N/N system is more sensitive against vibrations. The use of the better suited coaxial system is not possible, due to the lack of space. A proposed solution would be to construct a device, where the furnace consists of Pt N/N coils. These coils are wounded closely to the sample For this prupose the Pt N/N coil is used generally as a furnace. During the "shoot-time" it should be switched off and then it acts as a pick-up system. Hopefully such a system should have a much better sensitivity.

Concluding, the present system can be used for high temperature (RT $\lesssim$ T < 500°C) hysteresis measurements in fields up to 50 kOe. Anisotropy fields, where the derrivative d^2M/dt^2 versus H has to be measured, can only be determined if H_a is below 30 kOe. This technique is naturally much more sensitive against noise. For higher H_a values the above proposed system is under construction.

3) Nd-Fe-B magnets

This type of new magnets are, due to economical considerations, a great hope to develop a high quality low cost material. The generally used chemical composition is $Nd_{15}Fe_{77}B_8$, however it is believed that the real chemical formula is $Nd_2Fe_{14}B$. Structural investigations showed, that $Nd_2Fe_{14}B$ forms a tetragonal cell (a = 8,80 Å, C = 12,19 Å),

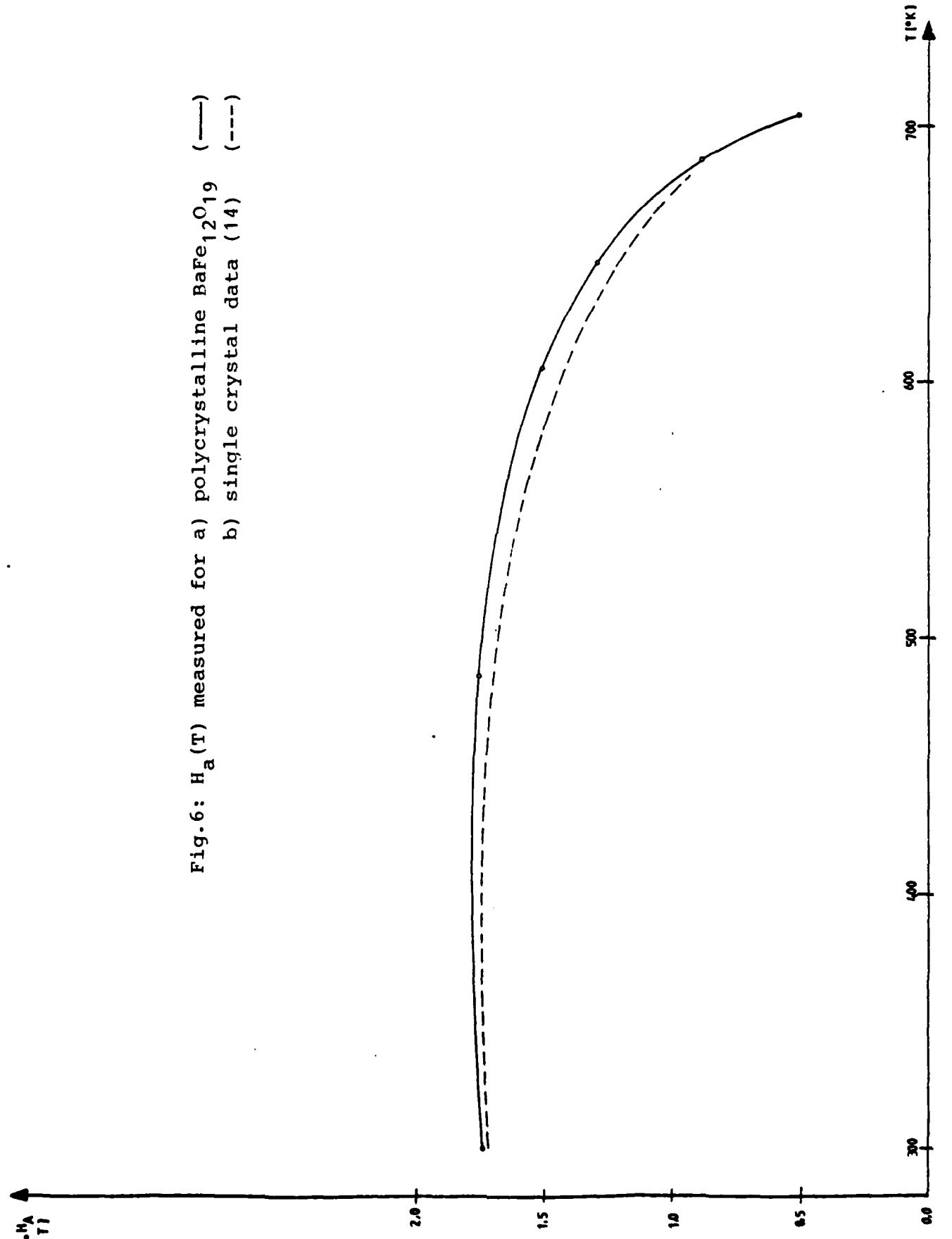

Fig.6: $H_a(T)$ measured for a) polycrystalline $BaFe_{12}O_{19}$ (——)
b) single crystal data (14) (- - -)

which belongs to the space group $P4_2/mnm$ (15). The theoretical density is 7,60 g/cm^3 which agrees well with the measured value of 7,55 g/cm^3. All $RE_{15}Fe_{77}B_8$ compounds were found to be uniaxial at room temperature except Sm, Er and Tm (16). Large energy products have been achieved only with Pr and Nd (17).

3.1) Magnet production

Two different producing methods exist:

i) $SmCo_5$ like: The material is melted and grinded to a powder of less then 10 μm. The powder is aligned and pressed perpendicular to the aligning field at a pressure of 200 MPa. The compacts were sintered in Ar-atmosphere at a temperature from 1310 - 1430 K for 1 h and then rapidly cooled. A post sintering heat treatment for 1 h at approximately 900 K is necessary in order to obtain a large coercivity (3). Energy products up to 40 MGOe are achieved with this method (4).

ii) Rapidly quenching technique (2): In this case the melt is sprayed through a nozzle on a rotating Cu-wheel, where the solidification occures. The surface velocity of the Cu-wheel determines the cooling rate and therefore the magnetic properties of the material. A surface velocity between 14 m/s and 19 m/s is necessary for good hard magnetic properties. This technique is well known for producing amorphous, soft magnetic ribbons (18). However for the Nd-Fe-B magnets a microcrystalline structure is necessary for optimal properties. It is obvious that with this technique only isotropic magnets can be produced. The achievable energy product is therefore much lower and approximately 14 MGOe only. Comparing the X-ray pattern of Nd-Fe-B materials produced as decribed by i) or ii) it is obvious that both materials are based on the same crystallographic structure. The effect of the rapidly quenching technique becomes visible in Fig. 7 a, b, c, where the X-ray line pattern (CrKα-radiation) is shown for as cast $Nd_{15}Fe_{77}B_8$ and of rapidly quenched material produced with a surface velocity of v = 14 m/s (b) respectively v = 28 m/s (c). Note the with

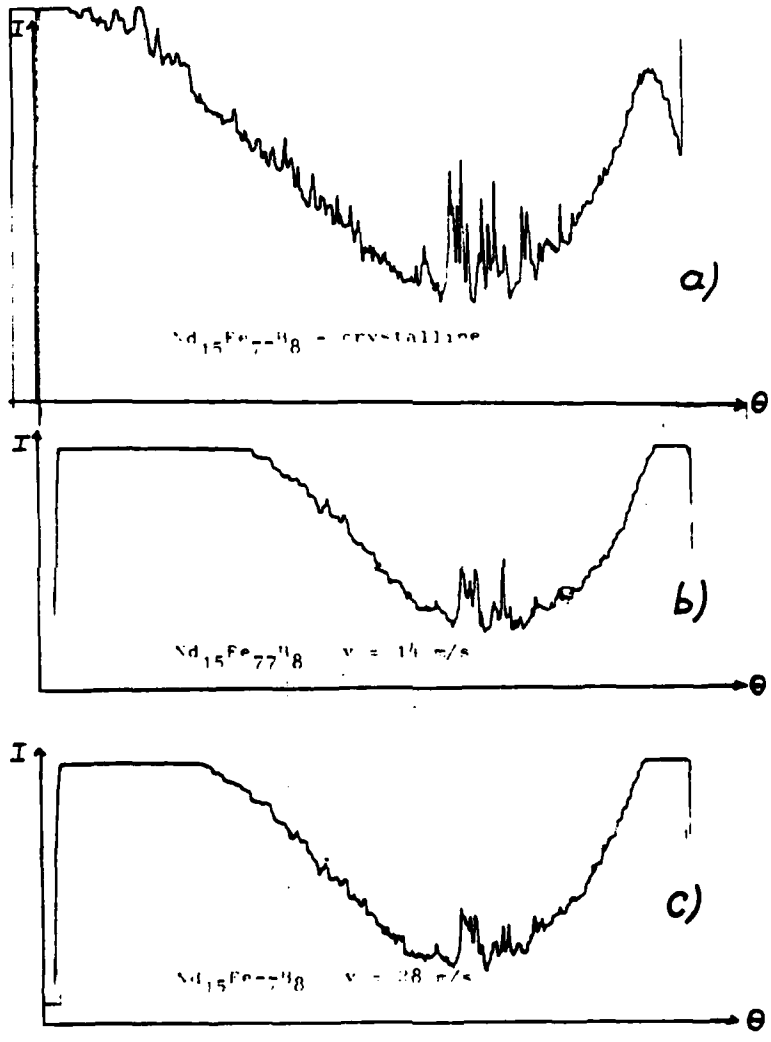

Fig.7: X-ray line pattern of $Nd_{15}Fe_{77}B_8$ for CrKα-radiation
Intensity as a function of θ
b) Rapidly quenched material; surface velocity v = 14m/s
c) Rapidly quenched material; surface velocity v = 28m/s

v decreasing intensities of the lines. Both production methods have the aim to form monodomainic particles. Concluding it can be said, that new high quality magnets, based on Nd-Fe-B can be produced. The magnetic data are: Saturation magnetization $4\pi M_s \sim 13$ kG, $_I H_c \sim 12$ kG, $(BH)_{max} \sim 30 - 40$ MGOe, $T_c = 300^{\circ}C$. The aim of the present work is to study the low temperature behaviour of these Nd-based magnets in order to get a better understanding of this new family of materials.

3.2) Anisotropy measurements

$Nd_{15}Fe_{77}B_8$ is uniaxial, the SPD-technique can therefore easily be applied, measuring $H_a(T)$ of polycrystalline samples. These measurements were performed on as cast $Nd_{15}Fe_{77}B_8$, rapidly quenched $Nd_{15}Fe_{77}B_8$ and as cast $Nd_2Fe_{14}B$. All samples were polycrystalline. Additionally aligned "Neomax" from Sumitomo Comp. was available. In order to study the Nd influence $Y_{15}Fe_{77}B_8$ was measured too. Table II summarieses the anisotropic fields as measured at room temperature (19).

Table II: H_a as measured at room temperature

sample	H (kOe)	remarks
$Nd_{15}Fe_{77}B_8$	78±5	as cast polycristalline
$Nd_{15}Fe_{77}B_8$	75±5	rapidly quenched
$Nd_2Fe_{14}B$	79	as cast polycristalline
Neomax	70	aligned
$Y_{15}Fe_{77}B_8$	25±1	as cast polycristalline

It is obvious that the anisotropy is determined by the $Nd_2Fe_{14}B$ structure, however it should be mentioned that one third of the anisotropy is caused by the Fe sublattice. The production technique seems not to be important for H_a at RT, Fig. 8 shows H (T) between 77 K and RT measured for the "Neomax" sample and the polycrystalline $Nd_{15}Fe_{77}B_8$. The different $H_a(T)$ leeds to the conclusion that the heat treat-

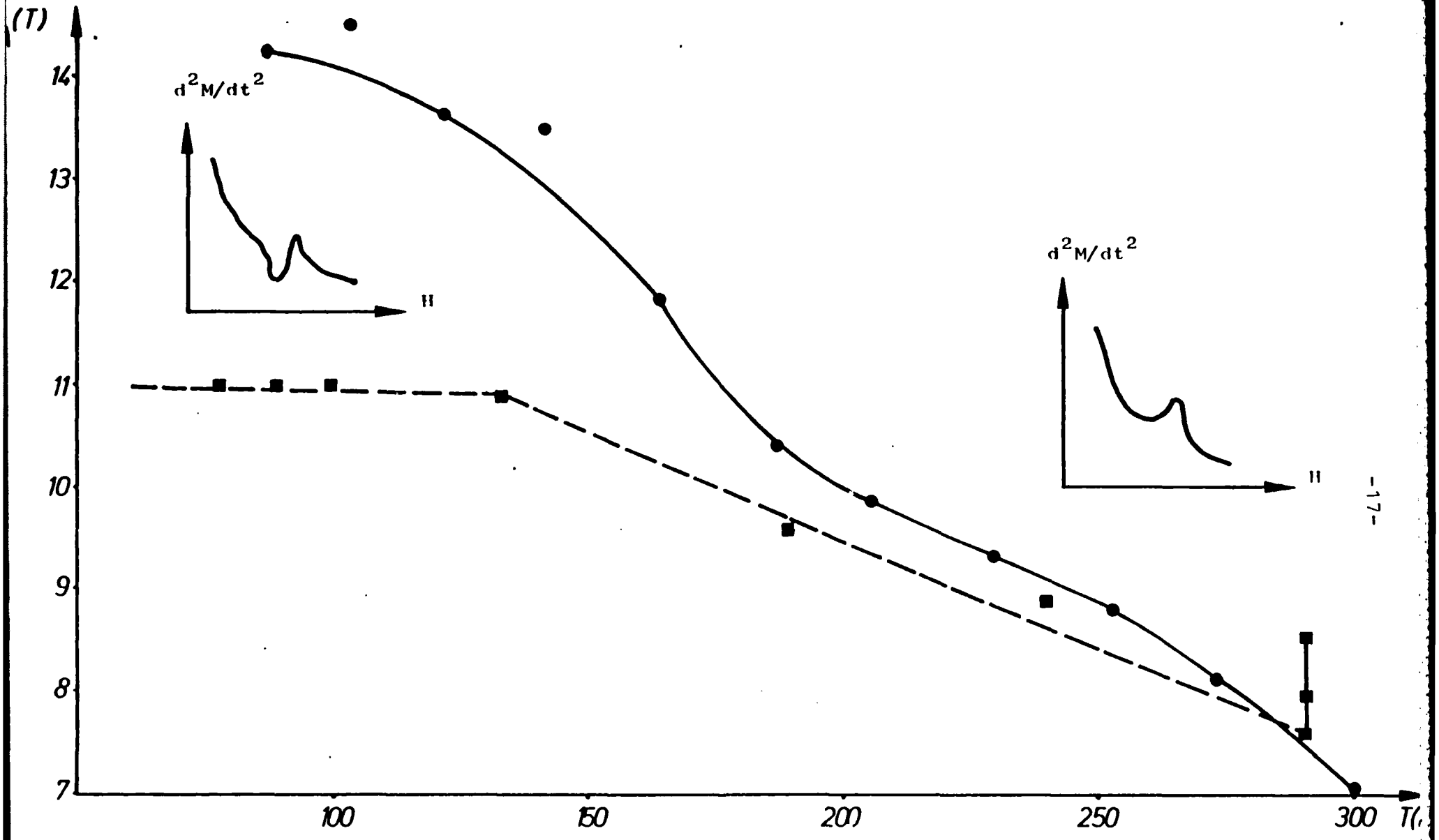

Fig.8: $H_a(T)$ measured for polycrystalline $Nd_{15}Fe_{77}B_8$ (■) and the "Neomax; sample (●).
The inserts show the changed character of d^2M/dt^2 vs H as measured above and below T^*

ment causes an atomic rearrangement, which is important for H_a. The fact, that the difference in $H_a(T)$ increases with decreasing temperature, gives a hint, that this rearrangement changes the crystal field mainly on the Nd positions. At approximatelx $T^* \sim 140$ K $H_a(T)$ shows a change of the slope. The inserts in fig. 8 show, how the measured d^2M/dt^2 versus H changes if $T < T^*$ or $T > T^*$ is valid. In fig. 9 as an example d^2M/dt^2 vs H for T = 300 K, fig. 10 the same for T = 135 K and fig. 11 the first derrivative dM/dt vs H at T = 135 K was plotted.

These pictures are looking similare as that obtained for $PrCo_5$. Fig. 12 shows dM/dt vs H at T = 77 K as measured on $PrCo_5$. For this material it is known, that it is uniaxial at RT, however for $T < 155^{\circ}K$ a FOMP transition occures (20). Below T = 107 K the first anisotropy constant becomes negative, an easy cone is therefore the easy axis of magnetization below T = 107 K. The situation becomes more clear, comparing the temperature dependence of the anisotropy constants. Fig. 13 shows K_1, K_2, K_3 as a function of the temperature as determined by (20). In fig. 14 $K_1(T)$ and $K_2(T)$ from the corresponding compounds YCc_5, $CeCo_5$ and $SmCo_5$ is drawn (21). $K_1(T)$ from YCo_5, which is between liquid He and RT nearly constant, and approximately $5 \cdot 10^7$ erg/cm^3 represents the anisotropy behaviour of the Co-sublattice. From fig. 13 it is visible, that $K_1(T)$ for $PrCo_5$ is of the same order of magnitude for $T > 150$ K. At $T \sim 150$ K, K_2 starts to increase and K_3, which is negative, increases too. There K_1 becomes unimportant, the anisotropy is mainly determined by the higher order constants. The mathematical analysis was given in more detail by (22). Fig. 15 presents $H_a(T)$ respectively $H_{cr}(T)$ measured down to 4,2 K which agrees well with (20). Even the downturn near the transition of H_a to H_{cr} can be understood by the temperature dependence of the anisotropy constants. It should be mentioned, that

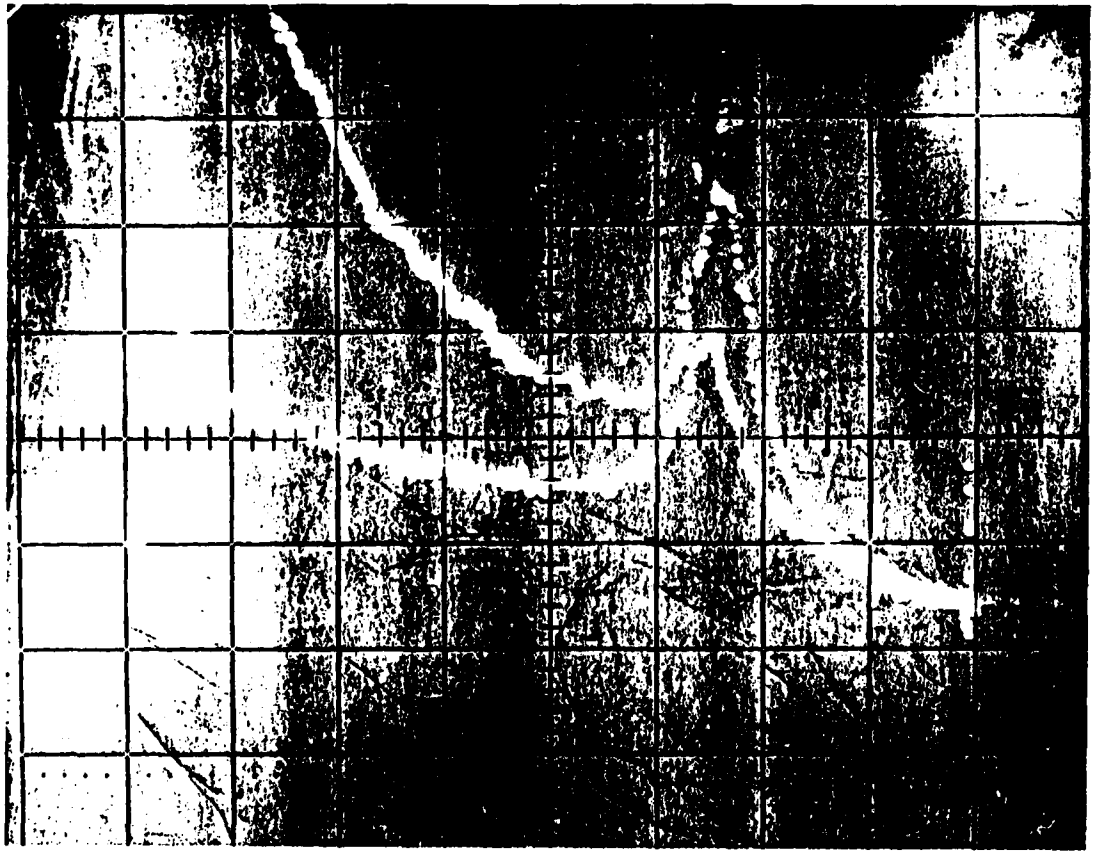

Fig.9: d^2M/dt^2 as a function of the field, measured on polycrystalline $Nd_{15}Fe_{77}B_8$ at T = 300 K

Fig.10: d^2M/dt^2 as function of the field, measured on polycrystalline $Nd_{15}Fe_{77}B_8$ at T = 135 K

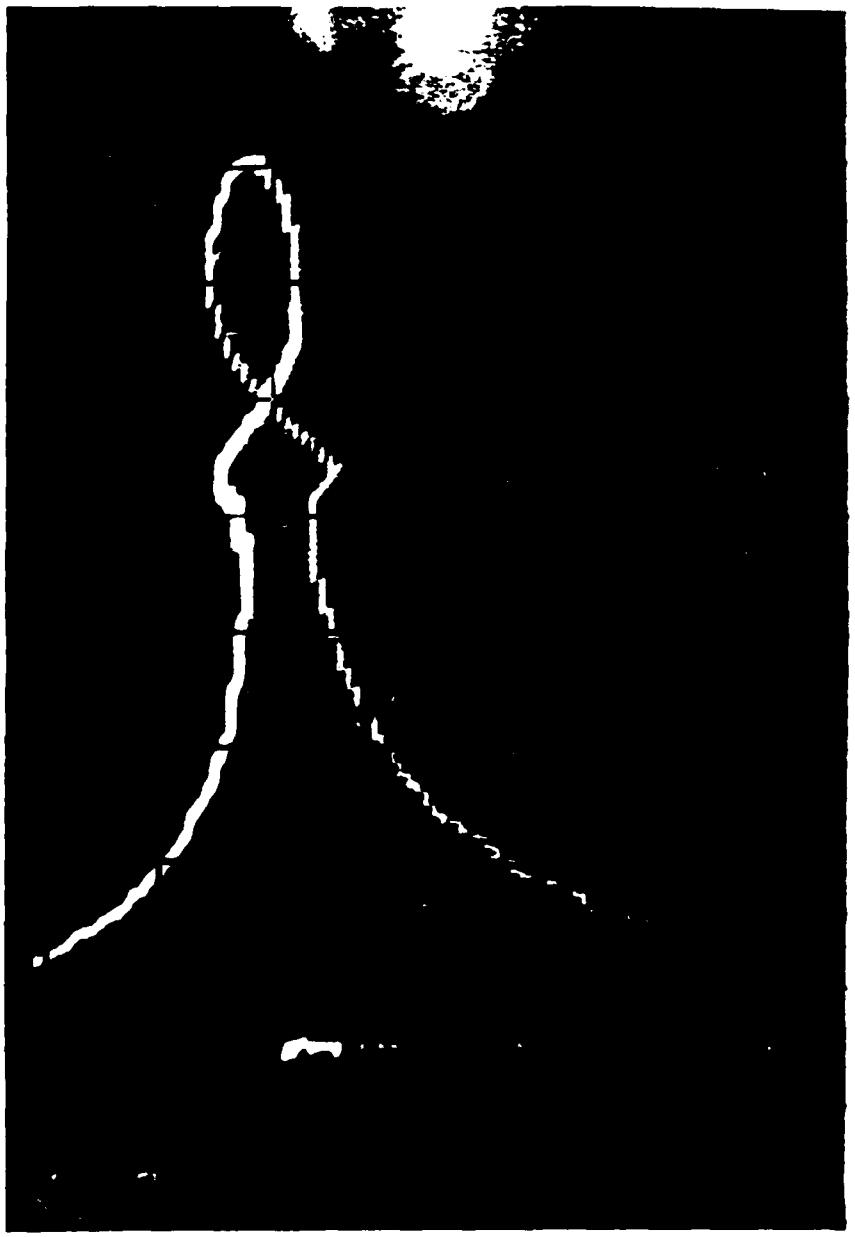

Fig.11: dM/dt as a function of the field measured on polycrystalline $Nd_{15}Fe_{77}B_8$ at T = 135 K

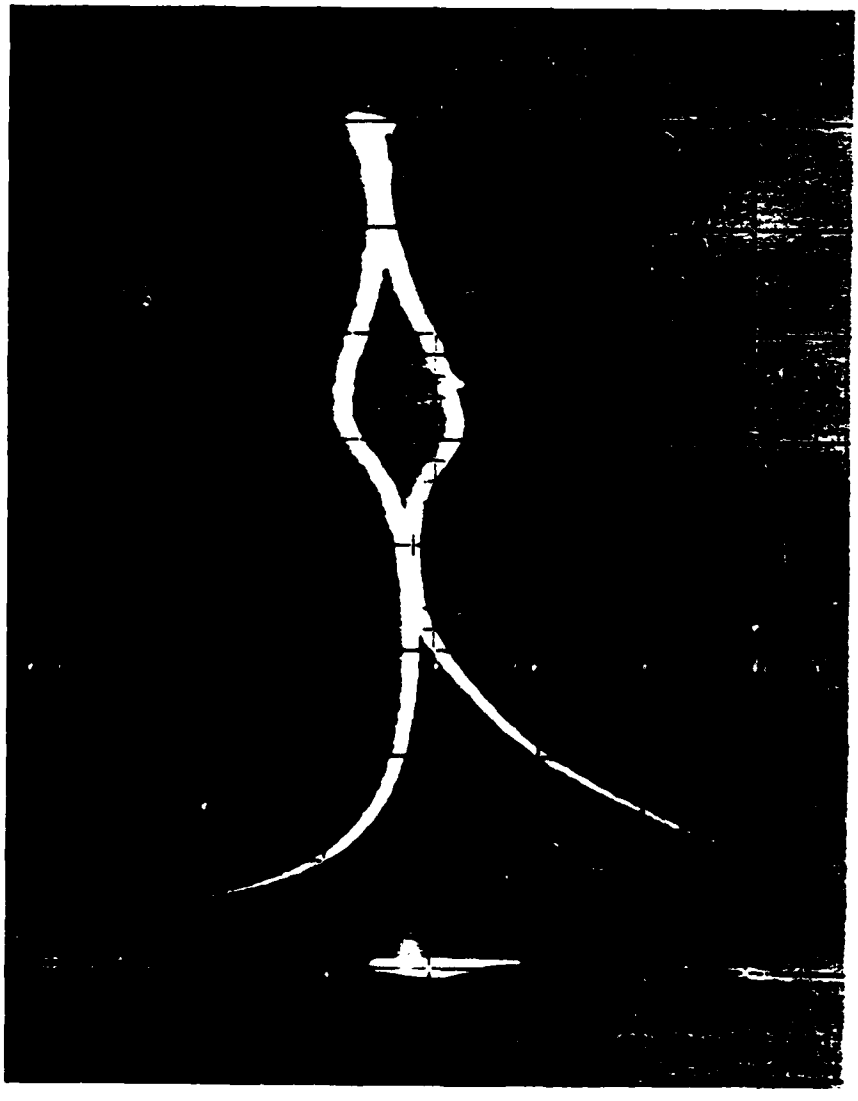

Fig.12: dM/dt versus H from $PrCo_5$ at T = 77 K

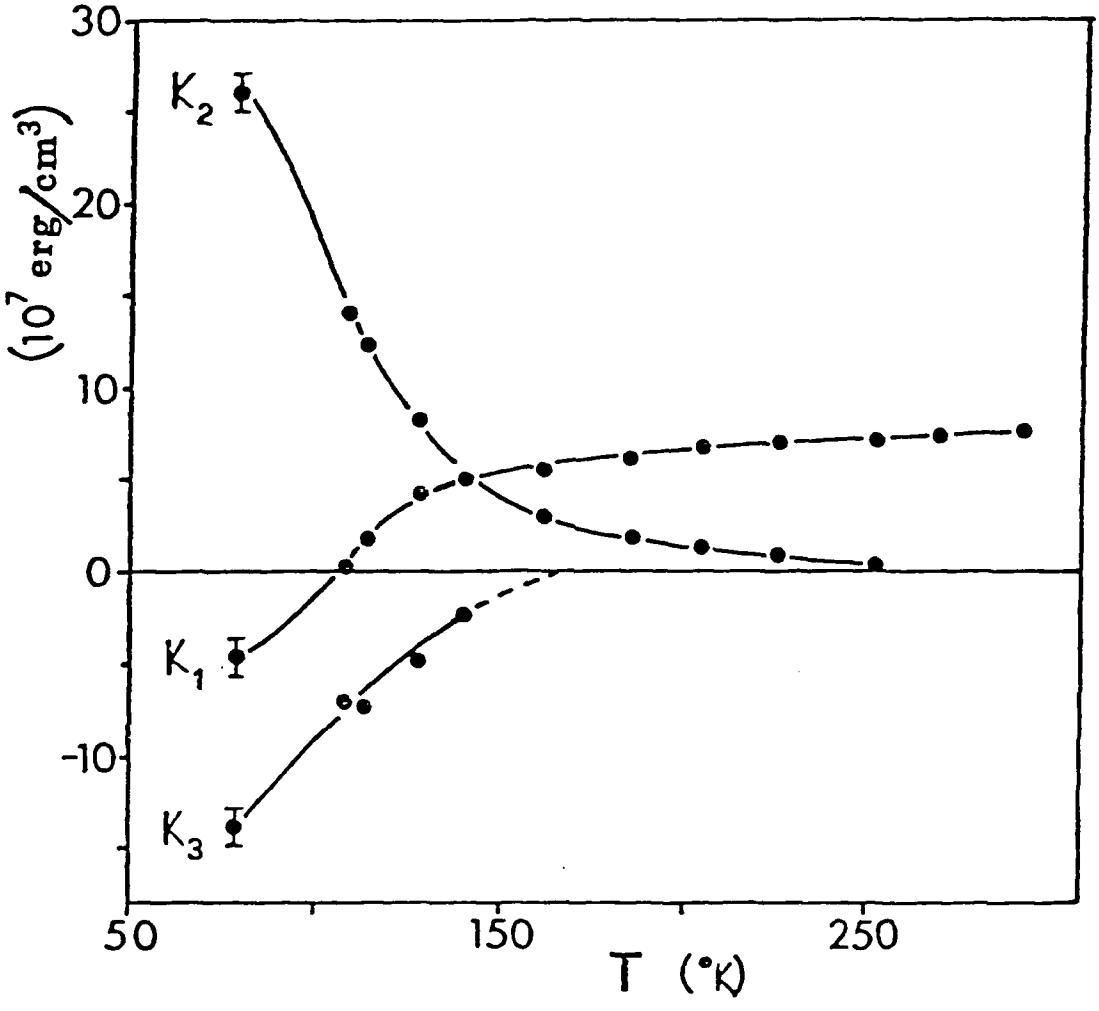

Fig.13: $K_1(T)$, $K_2(T)$ and $K_3(T)$ of $PrCo_5$ according to (20)

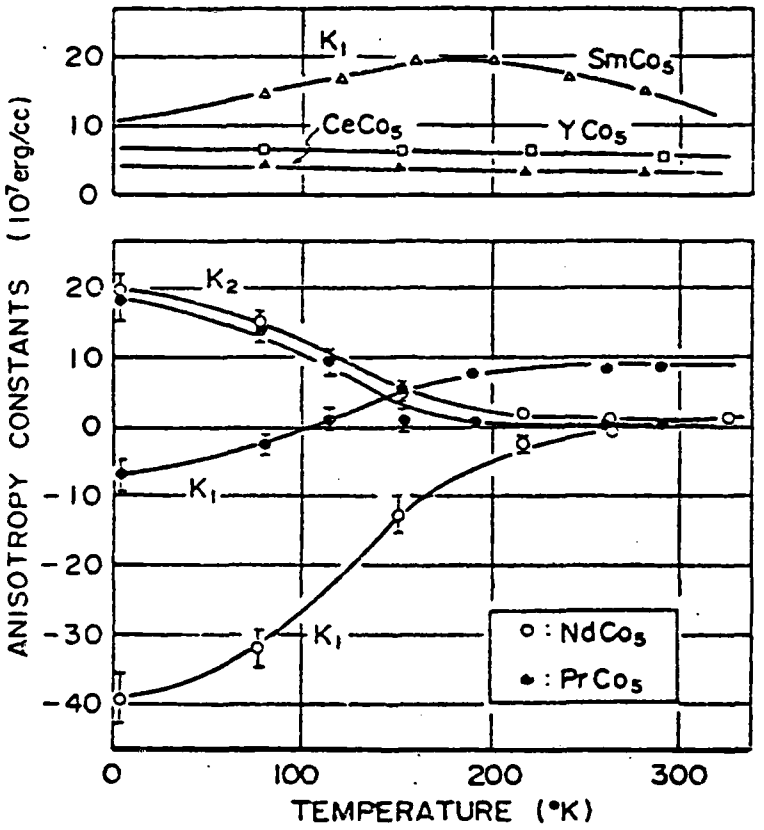

Fig.14: $K_1(T)$ and $K_2(T)$ for YCo_5, $SmCo_5$, $NdCo_5$ and $PrCo_5$ according to (21)

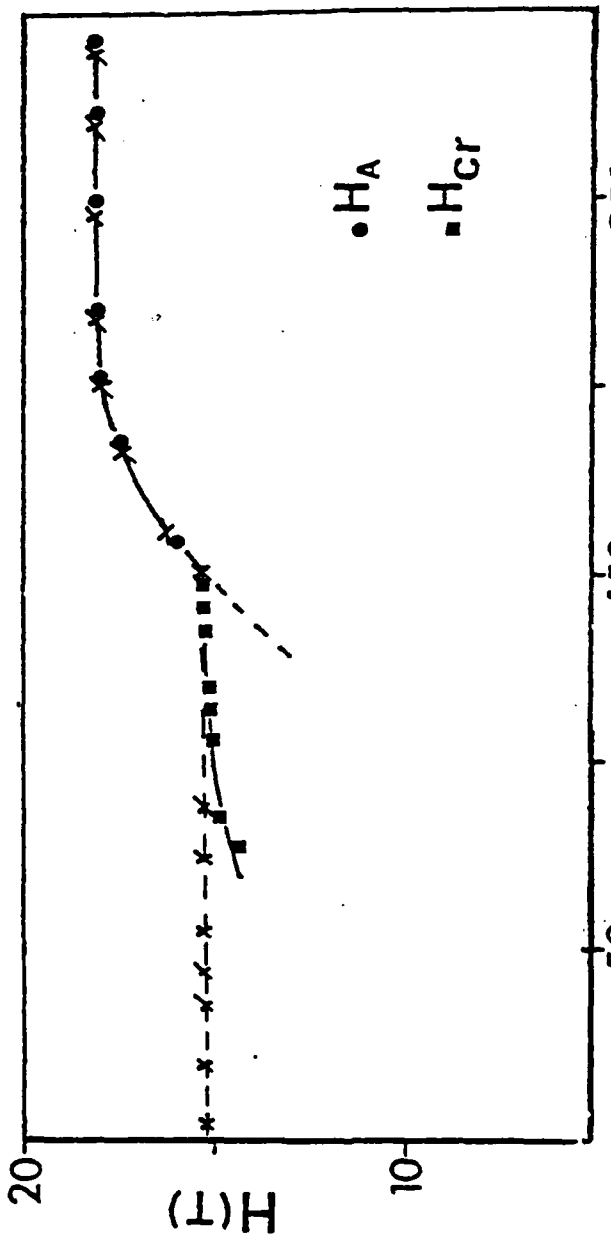

Fig.15: $H_a(T)$ (•) and $H_{cr}(T)$ (▪) of $PrCo_5$ due to own measurements (x) and according to (20)

$PrCo_5$ could be an excellent material for the field calibration at RT, because H_a is there nearly temperature independent. Additionally it was found, that H_a does not depend on the exact Pr-Co stoichiometry (20).

The analysis of $PrCo_5$ can be used to understand the low temperature behaviour of $Nd_{15}Fe_{77}B_8$. The corresponding compound $Y_{15}Fe_{77}B_8$ showed also a smooth $H_a(T)$ characteristic; $H_a(T)$ decreases slightly with decreasing temperature. For $Y_{15}Fe_{77}B_8$ no change of the d^2M/dt^2 vs H behaviour was detected.

3.3) Hysteresis measurements

At the "Neomax" sample first hysteresis measurements were performed. In fig. 16 and fig. 17 the M(H) loops at RT and T " 77 K as an example are given. In the loops kinks are visible which might indicate, that a second phase with a lower coercivity and a higher magnetization is present. Similar loops were published by (2) studying rapidly quenched Nd-Fe-B magnets with varying surface velocity. Our investigations on Nd-Fe-B magnets, produced with the same technology, gave also such unusual hysteresis loops.

From the hysteresis measurements, which were performed between 77 K and 300 K, the temperature dependence of the coercivity was obtained (see fig. 18). Note, that $H_c(T)$ is nearly linear, no anomaly near $T \sim 140$ K was detectable. The saturation magnetization was temperature independent for 77 K $\lesssim T \lesssim$ RT ($4\pi M_s \sim 11$ kG). In order to test, if a conus below T^* is detectable as a step in M(H) the high field magnetization at T = 77 K was measured in a field up to 150 kOe. Unfortunately no such step was measurable, M(H) looked smoth. Therefore no decision between FOMP or conus was possible. If a conus exists, the deflection angle must be small.

Fig.16: M(H) of "Neomax" at T = 300 K

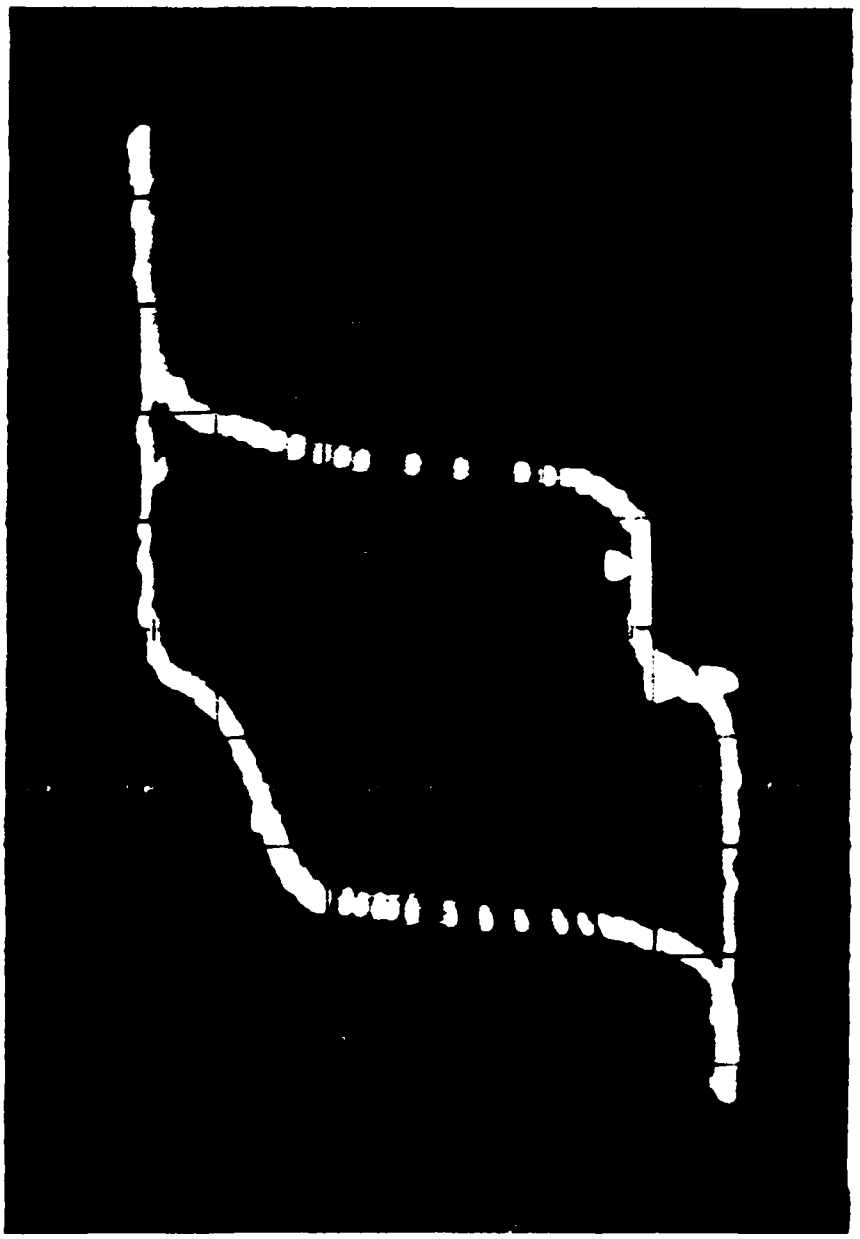

Fig.17: M(H) of "Neomax" at T = 77K

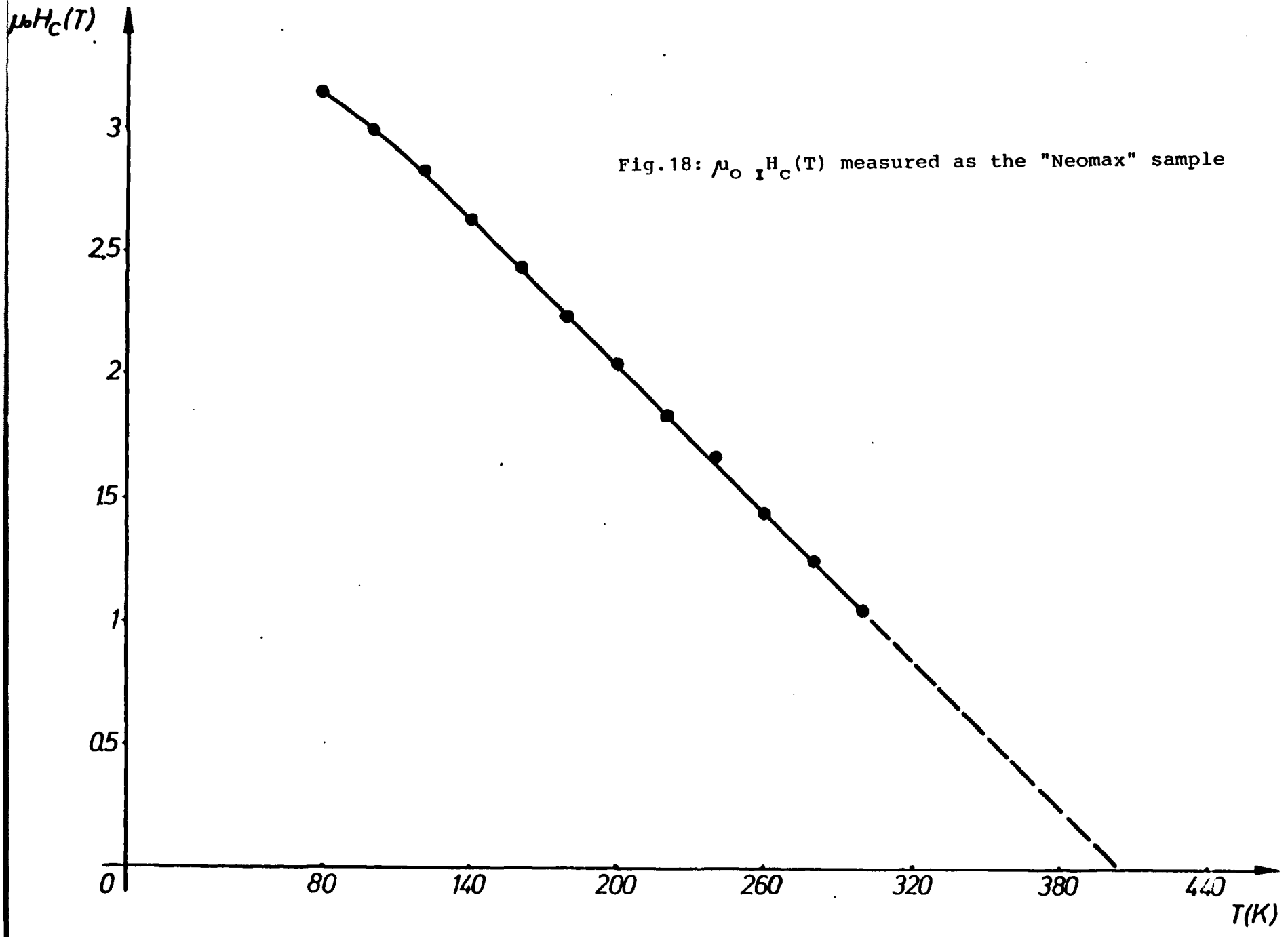

Fig.18: μ_o $_I H_c(T)$ measured as the "Neomax" sample

3.4) AC-susceptibility χ_i

The value of the AC-susceptibility was found to be very sensitive against any spin reorientation. This was proofed on various $RECo_2$ compounds (23). The reason is that χ_i is proportional to:

$$\chi_i \propto \frac{M_S^2}{\text{anisotropy + magnetoelast. energy}}$$

Therefore $\chi_i(T)$ was measured between 4,2 K and 300 K, applying an AC-field of 1,25 Oe (f = 82 Hz). In fig. 19 $\chi_i(T)$ of a polycrystalline $Nd_{19}Fe_{77}B_8$ sample and the Sumitomo magnet is plotted. In the case of a magnetized material χ_i represents the slope of the M(H) curve at the working point, which is given by the demagnetizing factor (sample dimensions 1x1x4 mm, H parallel to the long axis). Note, that $\chi_i(T)$ of the polycrystalline sample shows a cusp at $T^* \sim 140$ K. For $T > T^*$ χ_i for H_{ext} parallel to the c-axis is larger than for H_{ext} perpendicular to the c-axis. Below T^* the relative magnitude is quiet the reverse. For comparison we measured $\chi_i(T)$ for $PrCo_5$ too. In fig. 20 $\chi_i(T)$ of a polycrystalline $PrCo_5$ sample and a magnetized $(Sm_{0,5}\ Pr_{0,5})\ Co_5$ material is drawn. There $\chi_i(T)$ shows also a kink which is near to the temperature where the easy cone develops. At the temperature where the FOMP starts, no anomaly in $\chi_i(T)$ was detected. It is worth to note, that the relative magnitude of the $\chi_i(T)$ of the magnetized samples changes also for $T > T^*$ compared with $T < T^*$. This leads to the conclusion that this change of the relative magnitude at T^* reflects also the spin reorientation. The fact that $\chi_i(T)$ of $PrCo_5$ shows a cusp where the easy cone appears, but no anomaly where the FOMP transition starts, can be used as a hint that the cusp in $Nd_{15}Fe_{77}B_8$ represents a real spin reorientation. In $Y_{15}Fe_{77}B_8$ no such anomaly was detected.

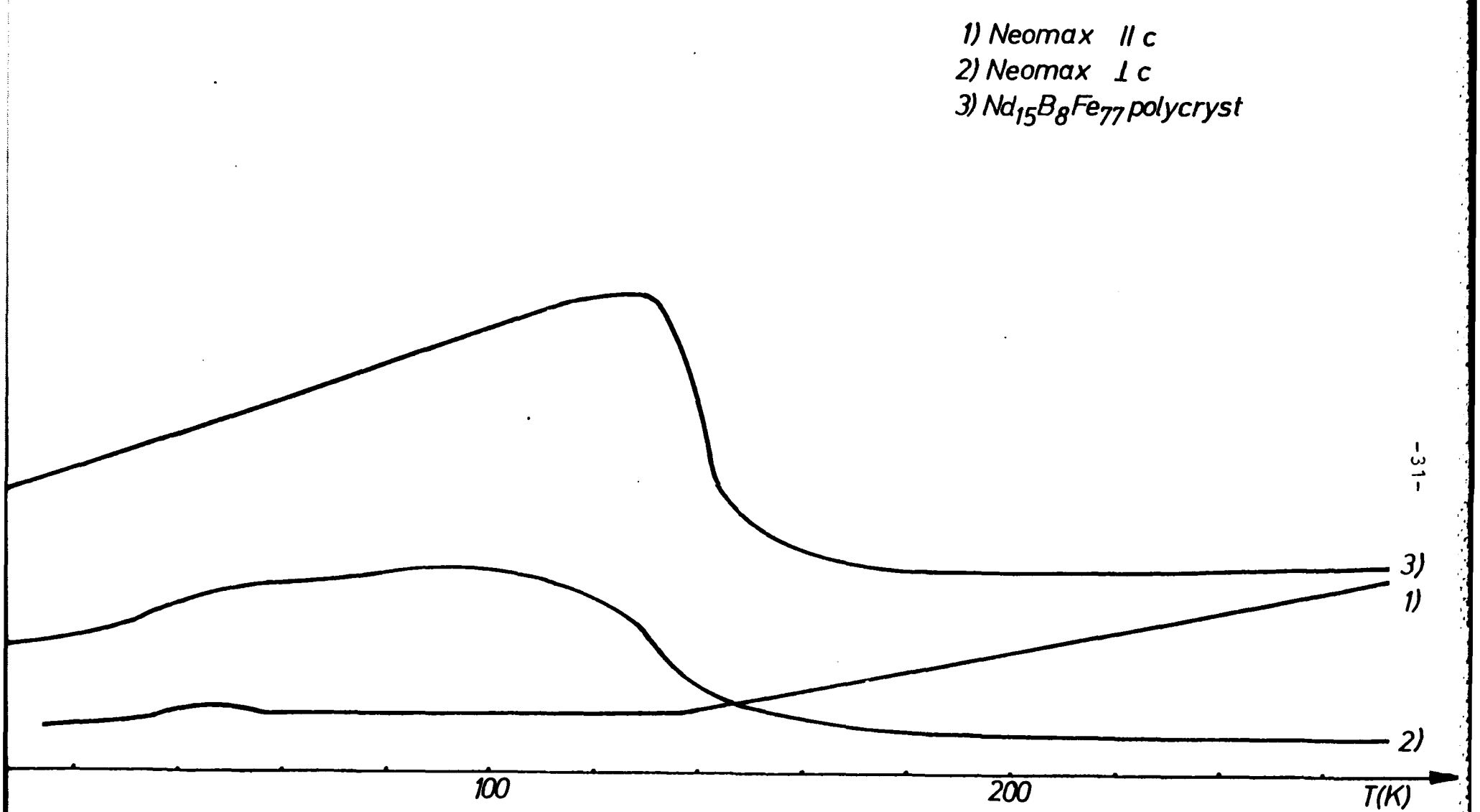

Fig.19: $\chi_i(T)$ of polycrystalline $Nd_{15}Fe_{77}B_8$ and the "Neomax" samples applying the field parallel respectively perpendicular to the c-axis

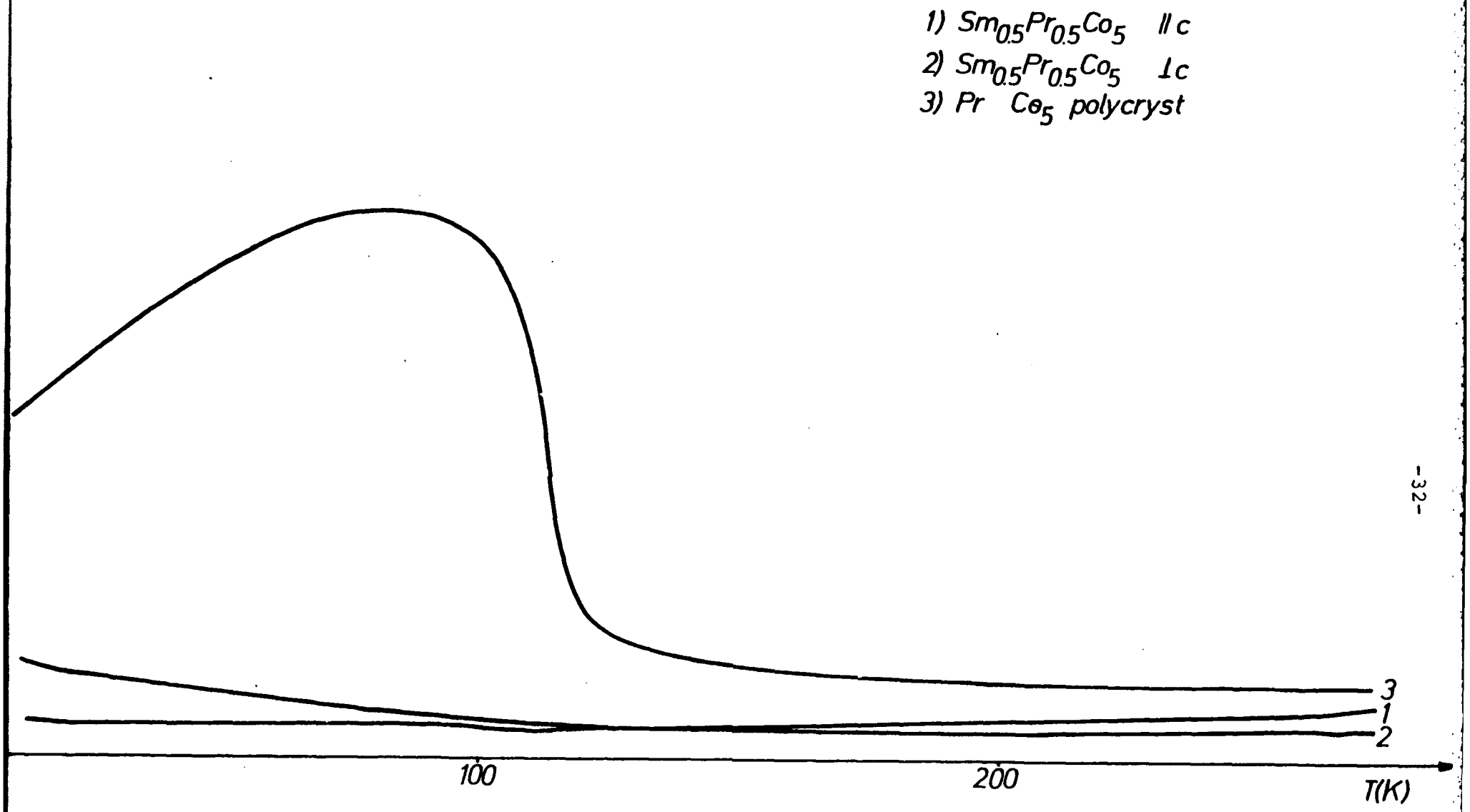

Fig.20: $\chi_i(T)$ of polycrystalline $PrCo_5$ and a $(Sm_{0,5}Pr_{0,5})Co_5$ magnet (sample 1 of table III) applying the field parallel respectively perpendicular to the c-axis

3.5) Thermal expansion

The thermal expansion of a magnetic sample consists always of a sume of lattice contribution plus a contribution resulting from the spontaneous volume magnetostriction. The magnetoelastic energy is therefore important for the thermal expansion $\Delta l(T)/l_o$. We measured the thermal expansion using a membran method (24) between 4,2 K and 300 K. The calibration was performed measuring $\Delta l(T)/l_o$ of pure elements like Ni. Fe, Co, Al, Cu and Nb taking the published data from (25) into account, for calculating the calibration functions.

Fig. 21 represents the thermal expansion of some polycrystalline $RECo_5$ compounds (RE = Sm, Nd, Pr). Note, that the $\Delta l(T)/l_o$ curve shows for $PrCo_5$ a kink at approximately T^*, which is the spin reorientation temperature. In fig. 22 $\Delta l(T)/l_o$ of the polycrystalline $Nd_{15}Fe_{77}B_8$ (curve C) as well as that of the magnetized Neomax samples is drawn, where the measuring direction was parallel (curve B) respectively perpendicular (curve A) to the aligning axis. It is obvious, that the thermal expansion of a magnetized sample can be expressed as:

$$\Delta l(T)/l_o = 1/l_o \left[(\Delta l)_{lattice} \pm \lambda(N) \right]$$

where $\lambda(N)$ describes a remanent magnetostrictive contribution, which is determined by the demagnetizing factor. There was no strong anomaly detectable in the $\Delta l(T)/l_o$ curve of the polycrystalline $Nd_{15}Fe_{77}B_8$ sample, indicating that the change of the magnetoelastic energy at T^* must be much smaller that in $PrCo_5$. The thermal expansion measured on the Neomax material exhibits a broad maximum near T^*, which might be correlated to the change of anisotropy at this temperature.

For comparison we plotted in fig. 23 and fig. 24 the thermal expansion of various $(Sm_{0,5}\ Pr_{0,5})Co_5$ magnets, where the heat treatment as given in table III was varied.

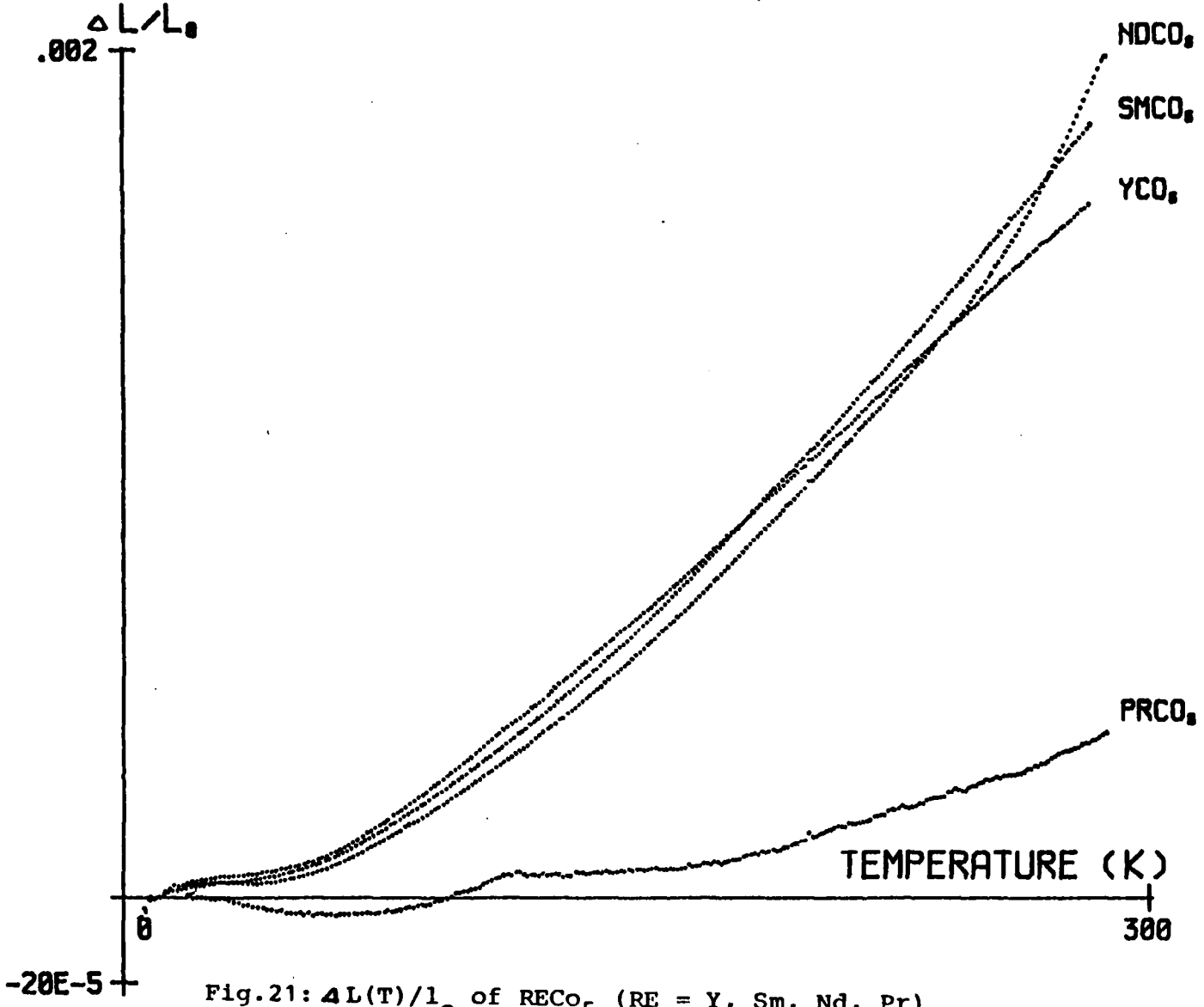

Fig.21: $\Delta L(T)/l_o$ of $RECo_5$ (RE = Y, Sm, Nd, Pr)

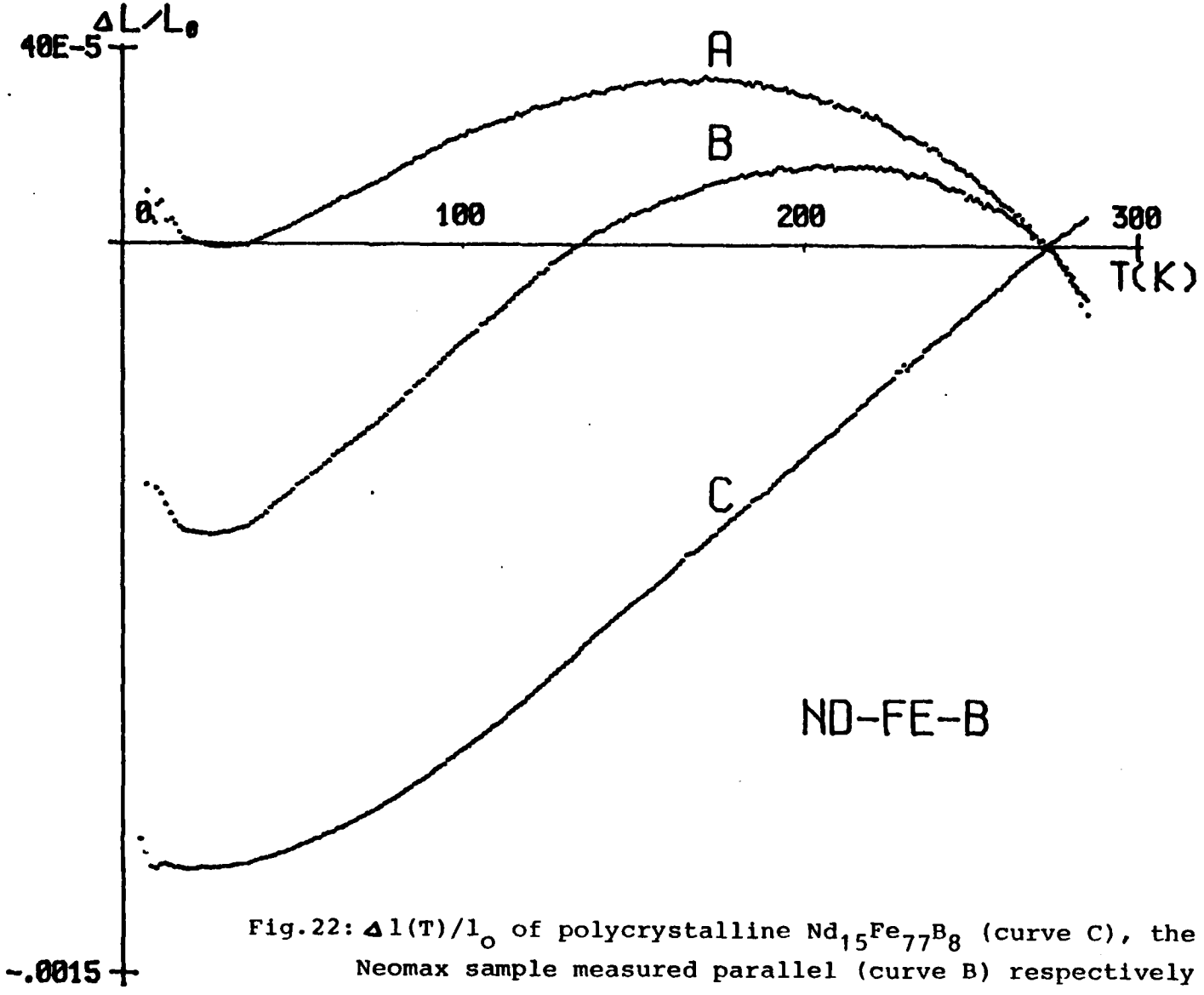

Fig.22: $\Delta l(T)/l_o$ of polycrystalline $Nd_{15}Fe_{77}B_8$ (curve C), the Neomax sample measured parallel (curve B) respectively perpendicular (curve A) to the c-axis

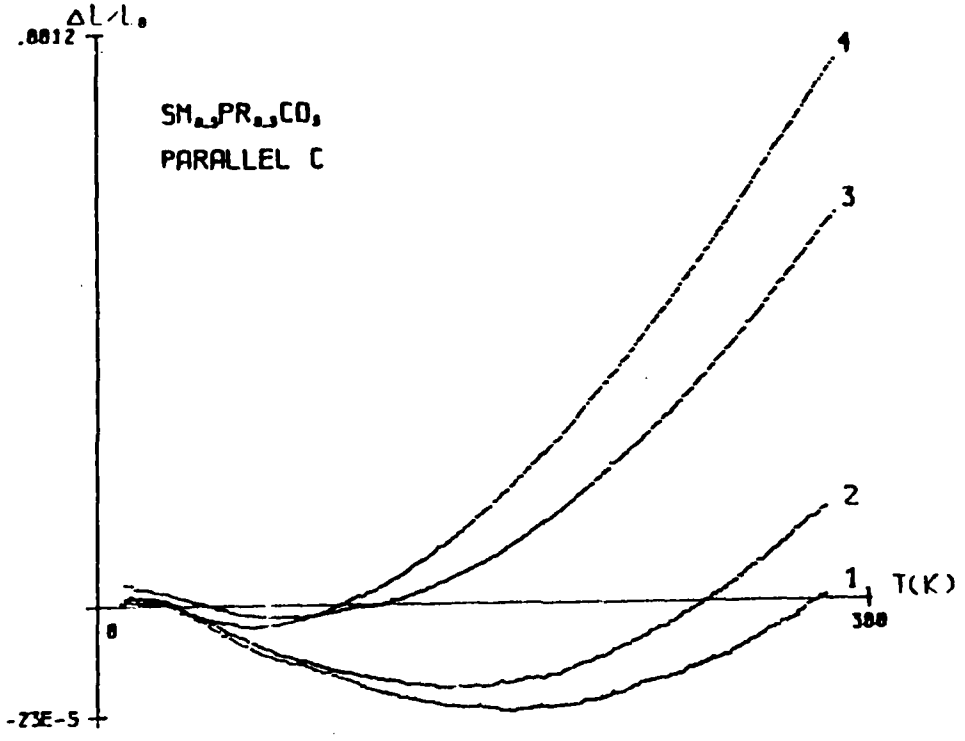

Fig.23: $\Delta l(T)/l_o$ of $(Sm_{o,5}Pr_{O,5})Co_5$ magnets measured parallel to the c-axis. The numbers indicate the thermal history (see table III) according to (9)

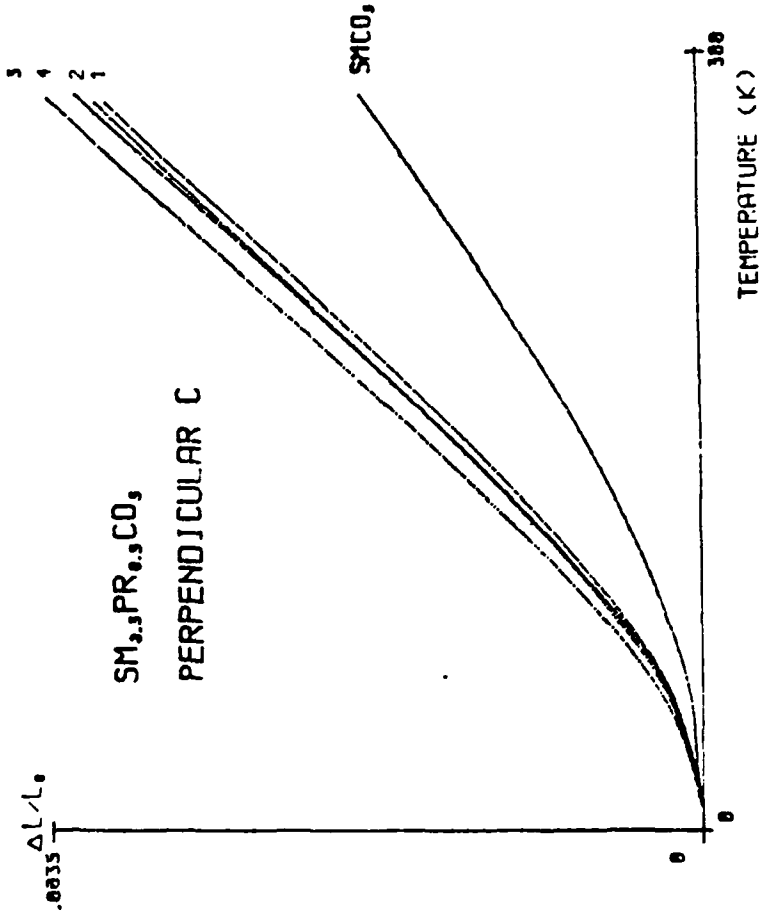

Fig.24: $l(T)/l_o$ of $(Sm_{0,5}Pr_{0,5})Co_5$ magnets measured perpendicular to the c-axis. The numbers indicate the htermal history (See table III) according to (9)

Fig. 23 represents $\Delta l(T)/l_o$ measured parallel to the c-axis, fig. 24 $\Delta l(T)/l_o$ as obtained perpendicular to the c-axis. It is easy to see, that a broad minimum in $\Delta l(T)/l_o$ (fig. 23) occurs, where the temperature of this minimum decreases with increasing duration of the sintering process. This indicates the difusion of the Sm-atoms into the $PrCo_5$ lattice as was discussed by (9). No anomaly is detectable in fig. 24.

These results show that the thermal expansion reflects generally a spin reorientation sensitively.

Table III: Heat treatment of the $(Sm,Pr)Co_5$ magnets

Sample	sintering temperature duration (K/min)	post-sintering heat treatment
1	1390/10 in vacuum	no post-sintering treatment
2	1390/10 under 800 mbar Ar	slowly cooled from 1320 to 1150 K in 1000 min
3	1390/20 under 800 mbar Ar	———"———
4	1390/30 under 800 mbar Ar	———"———

3.6) Conclusion

All low temperature measurements performed on the Nd-Fe-B material indicates, that the anisotropy changes its character at $T^* \sim 140$ K. Especially the comparison with $PrCo_5$, which shows a similar behaviour, gives the impression, that an easy cone with a small deflection angle developes at $T < T^*$. The reason for this spin-reorientation must be a change of the splitting of the crystal field levels of the Nd atoms in this structure. An absolute clear decision if a FOMP transition appears below T^*, or if really an easy cone developes is not yet possible. For this purpose single crystal measurements, or neutron diffraction experiments at low temperatures are necessary.

4) Proposed developments

4.1) Technical improvements

The technical development will be focused on the improvement of a high field, high temperature equipment. A solution of the high temperature pick-up troubles is in work.

The measuring sensitivity of the whole apparatus will be improved by the proposed use of a modern transient recorder. Attempts to link the measuring electronic to a personal computer would be performed in order to develop an easy to handle low cost pulsed field hysteresograph for industriel applications.

4.2) Scientific proposals

High temperature hysteresis measurements on commercial permanent magnets especially on that of Shin-Etsu are in preparation in order to study the technical range of interest. If the technical improvements are successfull, comparisons with $H_a(T)$ are planned.

Further investigations on the Nd-Fe-B magnets are also proposed. New samples from Sumitomo and Colt Ind. exist. Also there the interest will be focused now on the high temperature range.

Literature

1) J. Fiedler, R. Grössinger, H. Kirchmayr, P. Skalicky
Final Rep. of United States Army (1983)
Contract Number DAJA 73-82-C-0050

2) J. Croat, J.F. Herbst, R.W. Lee, F.E. Pinkerton
J. Appl. Phys. 55 (1984) 2078

3) M. Sagawa, S. Fujimura, M. Togawa, H. Yamamoto,
Y. Matsuura
J. Appl. Phys. 55(6) (1984) 2083

4) K.S.V.L. Narasimhan
Proc. of Intermag Conf. Hamburg (1984)

5) R. Grössinger
Proc. of VI Int. Workshop on Rare Earth-Cobalt Magnets
Baden/Vienna (1982) p. 305

6) P. Obitsch
Thesis Techn. Univ. Vienna (1984)

7) G. Asti, S. Rinaldi
J. Appl. Phys. 45 (1974) 3600

8) F. Rothwarf, Y. Tawara, K. Chashi, J. Fidler
P. Skalicky, R. Grössinger, H. Kirchmayr, S. Liu,
K.J. Strnat
Proc. of VI Int. Workshop on Rare Earth-Cobalt Magnets
Baden/Vienna (1982) p. 567

9) R. Grössinger, M. Velicescu
Proc. of VII Int. Workshop on Rare Earth-Cobalt Magnets
Beijing (China) (1983) p. 277

10) H.B. Callen, E. Callen
J. Phys. Chem. Solids 27 (1966) 1271

11) Xu Lai-Zi, Zhang Shu-Li, Cheng Yong-Shun, Yao Hong-Fu
Proc. V Int. Workshop on Rare Eartn-Cobalt Magnets
Roanoke (USA) (1981) p. 481

12) W. Hüning
Diplomarbeit, Ruhr Univ. Bochum (1976)

13) A. Arrot, J.E. Noaks
Phys. Rev. Lett. 19(14) (1976) 786

14) H.B.G. Casimir, J. Smit, U. Enz, J.F. Fast,H.P.J. Wijn, E.W. Gorter, A.J.W. Duyvesteyn, J.D.Fast, J.J. de Jong J. de Physique et le radium 20 (1959) 360

15) J.F. Herbst, J.J. Croat, F.E. Pinkerton, W.B. Yelon Phys. Rev. B 29(7) (1984) 4167

16) M. Sagawa, S. Fujimura, H. Yamamoto, Y. Matsuura, M. Miraga Proc. of Intermag Conf. Hamburg (1984)

17) J. Croat, J.F. Herbst, R.W. Lee, F.E. Pinkerton Appl. Phys. Lett. 44 (1984) 148

18) F.E. Luborsky Ferromagn. Mat. Ed. E. P. Wohlfarth North Holl. (1980) Vol.1 Chapt. 6, P. 451

19) F. Grössinger, P. Obitsch, X.K. Sun, F. Rothwarf, R. Eibler, H.R. Kirchmayr Mat. Science (1984) to be published

20) G. Asti, F. Bolzoni, F. Leccabue, R. Panizzieri, L. Pareti, S. Rinaldi JMMM 15-18 (1980) 561

21) E. Tatsumoto, T. Okamoto, H. Fuji, C. Inoue J. Physique 32 (1971) 551

22) G. Asti, F. Bolzoni JMMM 20 (1980) 29

23) R. Grössinger, G. Hilscher, H.R. Kirchmayr Microchem. Acta Suppl. 9 (1981) 161

24) R. Grössinger, H. Müller Rev. Scient. Instr. 52(10) (1981) 1528

25) A.S. Touloukian, R.K. Kirby, R.E. Taylor, P.D. Desai "Thermal Expansion Metallic Elements and Alloys" Thermophysical properties of Matter Vol. 12 IF II Plenum N.Y. (1977)

B) ELECTRON MICROSCOPE STUDY OF THE MICROSTRUCTURE OF RARE EARTH PERMANENT MAGNET MATERIALS

by

J. Fidler and P. Skalicky
Institute of Applied and
Technical Physics,
Technical University of Vienna
Karlsplatz 13,
A-1040 Vienna, Austria.

B.1. Introduction:

Permanent magnets with highest coercive forces are based on rare-earth intermetallic compounds. In the "single phase" $RECo_5$ sinter magnets the coercivity is determined by the nucleation field and expansion field of reversed domains [1,2]. In the precipitation hardened "multi-phase Sm_2Co_{17} "sinter magnets the high coercive force is obtained by the pinning of magnetic domain walls at the cell boundaries of a continuous precipitation structure [1,3]. The microstructure predominantly determines the origin of high coercive forces, i.e. the nucleation and expansion of reversed domains and the pinning of domain walls. Electron microscopic studies of the microstructure and the domain structure of rare earth permanent magnet materials provides a better understanding of the magnetic properties.

During the period Jan. 1984 - June 1984 two types of rare earth permanent magnet materials were investigated:

percipitation hardened Er-containing "multi-phase Sm_2Co_{17}" magnets and Nd-Fe-B magnetic materials.

B.2 Electron microscopy of $SmEr(Co,Fe,Cu,Zr)_{7.2}$ magnets

Copper containing cobalt rare earth magnets with a composition of $Sm(Co,Cu,Tm)_{6-8}$ with Tm = Zr, Ti,Hf show a fine cell morphology [3]. The electron micrographs show the rhombic cells of the

type $Sm_2(Co,Fe)_{17}$ which are separated by a $Sm(Co,Cu)_5$ cell boundary phase. In magnets with high coercivities ($>$1000 kA/m) thin plates were found perpendicular to the hexagonal c-axis. Our high resolution electron microscope investigations show that the crystal structure of the platelet phase is close to the hexagonal Sm_2Co_{17} structure, which is in agreement with metallurgical considerations [4]. We found that maximum coercivities occured in magnets with cell diameters of about 200 nm. Our Lorentz electron microscope investigations show that in the precipitation hardened "multi-phase Sm_2Co_{17}" magnets the magnetic domain walls are pinned at the cell boundary phase, which is in agreement with micromagnetic considerations [1].

For many applications of the multi-phase "Sm_2Co_{17}" magnets a high coercive force and a wide temperature range constancy of the magnetization is important. High coercive forces are obtained after an optimum post-sintering heat treatment of the magnets. The constancy of magnetization is obtained by partial subsitution of erbium for samarium [5]. A series of samples was made at the University of Dayton in an attempt to fulfill both of the foregoing requirements. Three samples with different chemical composition according to

$$Sm_{1-x}Er_x(Co_{.69}Fe_{.22}Cu_{.08}Zr_{.02})_{7.22}$$

with x = 0.0 (#1), 0.2 (#2) and 0.3 (#3)

TABLE I : Cell size parameters of the rhombic cellular microstructure parallel ($l_{//}$) and perpendicular ($l_{\perp}$) to the hexagonal c-axis, the density of the platelet phase (measured // to the c-axis) and the magnetic parameters of $SmEr(CoFeCuZr)_{7.2}$ magnets.

magnet #	$l_{\perp}$ [nm]	$l_{//}$ [nm]	Θ	number of platelets // c	$_{M}H_{c}$ [kOe]	B_r [kG]	$(B.H)_{max}$ [MGOe]
1	160	320	54^{o}	33/µm	15	10.6	25.8
2	170	400	46^{o}	35/µm	14.3	10.1	22.3
4	130	200	66^{o}	38/µm	10.6	9.9	20.9

have been investigated by means of transmission electron microscopy.

Figures 1,2 and 3 show the cellular microstructure of magnets #1, #2 and #3. The parameters of the rhombic cells, the density of the platelet phase and the magnetic parameters are summarized in table I. Figure 1b is a bright field image and shows the twinning within the cell interior phase. The twins were observed in all of the three samples. The size of the twins is found to be between 20-170 nm parallel to the c-axis. The platelet phase occured in all of the three samples, whereby the density of the platelets slightly increased with increasing Er-content. The cell size parameter parallel to the c-axis is in the case of magnet #1 $l_{\parallel}$ = 320 nm, leading to a very high intrinsic coercive force ($\gg$ 15 kOe). In the magnet #2 and #4 $l_{\parallel}$ was found to be 400 nm and 200 nm, respectively. Both magnets show a lower intrinsic coercive force than magnet #1, which is obviously due to the fact that the optimum cell size was not obtained in samples #2 and #4 after the post-sintering heat treatment.

B.3. Electron microscopy and x-ray microanalysis of Nd-Fe-B magnets

Two types of rare earth-iron permanent magnets can be distinguished. Magnets derived from rapidly solidified ribbons can be understood as

small-particle magnets (particle size ~ 50 nm). Such magnets obtain intrinsic coercivities up to 15 kOe and energy density products up to 20 MGOe [6]. Cast and sintered alloys with a chemical composition near $Nd_{15}Fe_{77}B_8$ exhibit a particle size up to 15 μm. Cast and sintered magnets exhibit intrinsic coercive forces up to 12 kOe and energy density products up to 45 MGoe [7,8]. Similar to the so called "single phase" $RECo_5$ magnets the coercive force of the rare-earth-iron-boron cast and sintered magnets is determined by the nucleation and expansion field of reversed domains. Depending on the Nd- and B-concentration different phases have been observed in such magnets by means of x-ray diffraction and electron diffraction, so far [8,9].

Nd-Fe-B magnets with a chemical composition $Nd_{15+x}\ Fe_{77-x}\ B_8$, with x = 0,1 and 2 and $Nd_{15.5}\ Fe_{66.5}\ Co_{10}\ B_8$,

supplied by various producers (SUMITOMO Spec.Met., SHIN-ETSU Chem. Corp. and VACUUM-SCHMELZE Hanau), were investigated by means of transmission electron microscopy and x-ray microanalysis.

In all of the different magnets three types of phases have been detected. The electron micrograph of fig.1a shows a typical grain boundary

junction of three grains, each with different chemical composition (figs. 4b,c and d). Grain A, which is always found to be free of crystal lattice defects, corresponds to the hard magnetic boride $Nd_2Fe_{14}B$ with a tetragonal crystal structure (a = 0.88 nm and c = 1.22 nm). Grain B, which is Nd-richer than grain A, corresponds to a tetragonal phase close to $NdFe_4B_4$ (a = 0.71 nm and c = 2.76 nm) 9,10. The grain interior of this phase shows a high crystal defect density. Under various reflections different crystal lattice defects such as dislocations, antiphase boundaries and stacking faults are visible (fig. 5a). The high resolution electron micrograph (fig. 5b) shows a fringe contrast corresponding to crystal lattice planes with a crystal lattice parameter of 4.8 nm. The grain boundary inclusion C is found to be a Nd-rich phase. Contrary to investigations by Stadelmaier et.al.[9], we did not only find Debye-Scherrer rings corresponding to a ß-Nd phase in the electron diffraction pattern of the phase C. In agreement with the investigations by Stadelmaier et.al.[9]we did also not detect phases corresponding to α-Fe, $Fe_{17}Nd_2$ and Fe_2Nd. The magnetic multi-domain structure within the grain A is shown in the Foucault micrograph of fig.6.

B.4 Future investigations

During the next six month-period we will continue the investigations according to our work plan for 1984:

(a) Quantitative analysis of precipitation hardened magnets of the type $Sm(Co,Fe,Cu,Zr)_{7.5}$ as provided by the Shin-Etsu Company. This will be done using high resolution electron microscopy and x-ray microanalysis to clarify the role of the Sm_2Co_{17}-based phases present in the enhancement of magnetic coercivity which occurs on ageing the material at an optimum temperature.

(b) Start the analysis of the microstructure of "single phase" $(PrSm)Co_5$ magnets. Transmission electron microscopy and x-ray microanalysis should compare the microstructure of Pr-containing magnets with the one of sintered $SmCo_5$ magnets.

B.5. List of papers submitted for publication

(1) J. Fidler and P. Skalicky: "On microstructure and coercivity of rare-earth permanent magnets."
Proc. of INTERMAG-Conference, Hamburg 1984.

(2) J. Fidler, P. Skalicky, M. Sagawa and Y. Matsuura: "Electron microscopy of Nd-Fe-B Magnets (NEOMAX 35)." Proc. 8th European Congress on Electron Microscopy, Budapest 13-18 August 1984.

REFERENCES

(1) H. Kronmüller, Proc.7th Int.Workshop RE-Co Perm.Magn., Beijing 1983, p.339.

(2) J. Fidler, Phil.Mag. B46, 565(1982).

(3) J. Fidler, P. Skalicky and F. Rothwarf, IEEE Trans.Magn. MAG-19, 2041(1983).

(4) A.E. Ray, Proc.7th Int.Workshop RE-Co Perm.Magn., Beijing 1983, p.261.

(5) H.A. Leupold, E. Potenziani, A. Tauber, H.F. Mildrum, J.Appl.Phys.55(1984) 2047.

(6) R.W. Lee, Proc.Intermag 84 - Conference, Hamburg 1984.

(7) M. Sagawa, Proc. Intermag 84 - Conference, Hamburg 1984.

(8) K.S.V.L. Narasimhan, Proc. Intermag 84 - Conference, Hamburg 1984.

(9) H.H. Stadelmaier, N.A. Elmasry, N.C. Liu and S.F. Cheng, Mat. Letters, in print.

(10) N.F. Chaban, Yu.B. Kuzma, N.S. Bilonizhko, O.O. Kachmar and N.U. Petrov, Dopov.Akad. Nank URSR Ser.A., Fiz.-Mat.Tekh.Nanki No.10 (1979) 873.

FIGURE CAPTIONS

Fig.1: Transmission electron micrographs showing the cellular microstructure of the precipitation hardened $SmEr(CoFe\ CuZr)_{7.2}$ magnet #1. (a) shows the platelet phase perpendicular to the c-axis and (b) shows the twinning within the cell interior phase.

Fig.2: Electron micrograph of the precipitation hardened $SmEr(CoFe\ CuZr)_{7.2}$ magnet #2.

Fig.3: Electron micrograph of the precipitation hardned $SmEr\ (Co\ Fe\ Cu\ Zr)_{7.2}$ magnet #4.

Fig.4: Electron micrograph and x-ray spectra of a $Nd_{15}Fe_{77}B_8$ sintered magnet. (a) shows three phase A,B and C. A is the hardmagnetic phase $Nd_2Fe_{14}B$ and is free of crystal lattice defects. B corresponds to a phase close to $NdFe_4B_4$ and C is the Nd-rich sintering phase. (b), (c) and (d) show the x-ray spectra of the phases A,B and C, respectively.

Fig.5: The phase B (Nd-richer than A) show a high defect density. (a) shows antiphase boundaries and stacking faults within the grain interior. (b) is a high resolution electron micrograph and shows a fringe contrast corresponding to a lattice plane spacing of 4.8 nm.

Fig.6: Foucault micrograph showing the magnetic domain structure within the hard-magnetic phase A. The foil-normal is parallel to the easy axis. There is no interaction with crystal lattice defects.

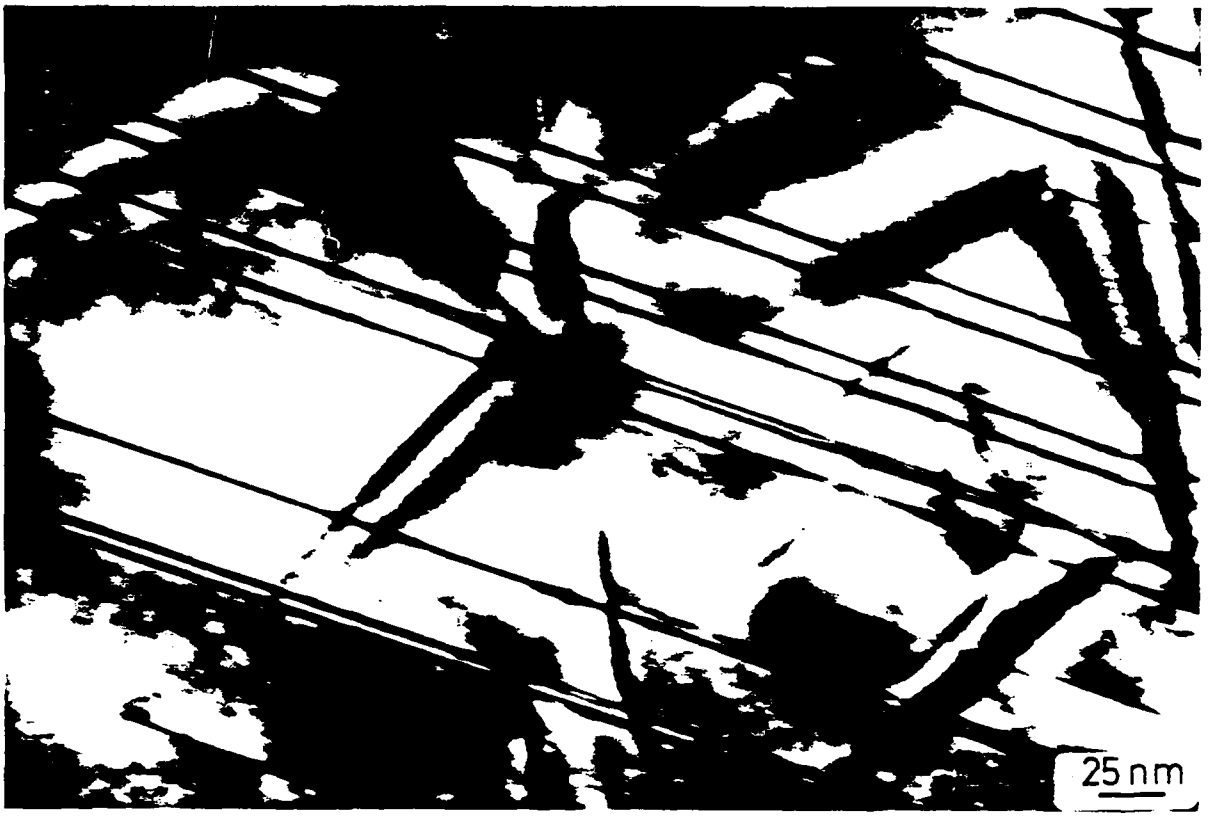

Fig.1a

Fig.1b

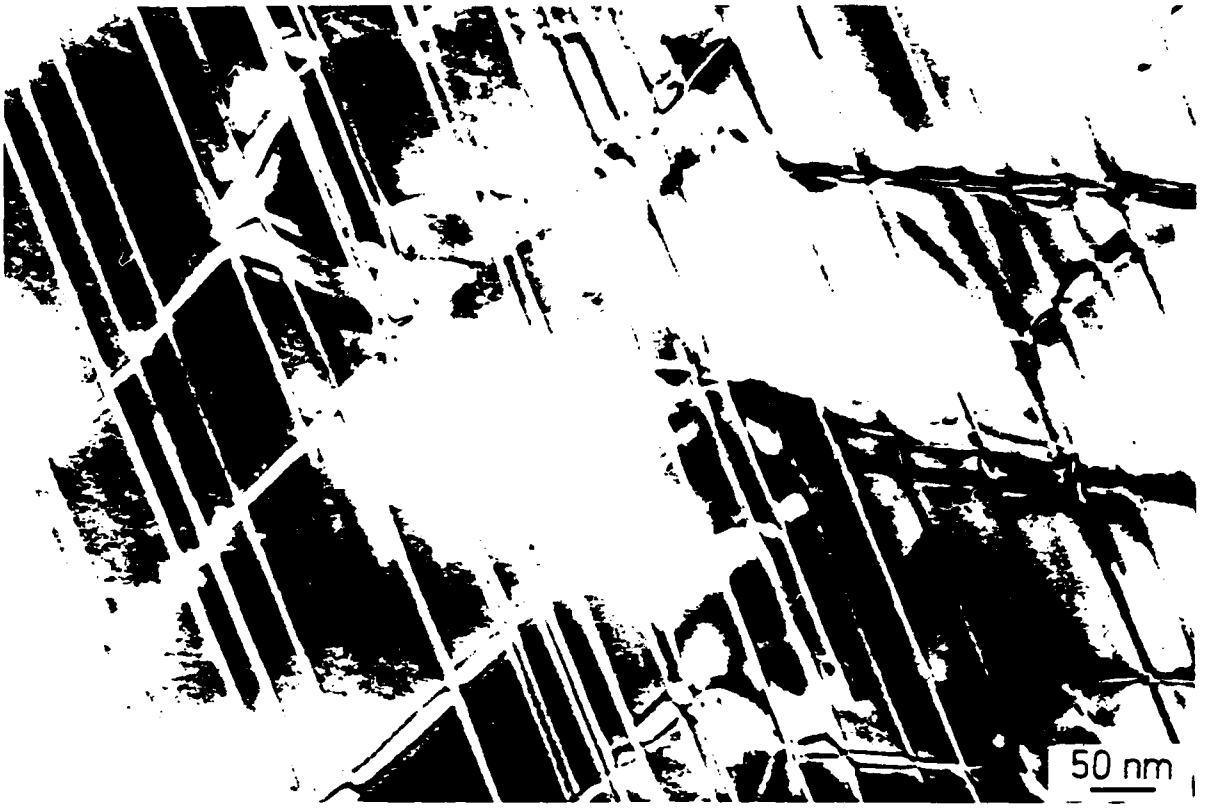

Fig.2

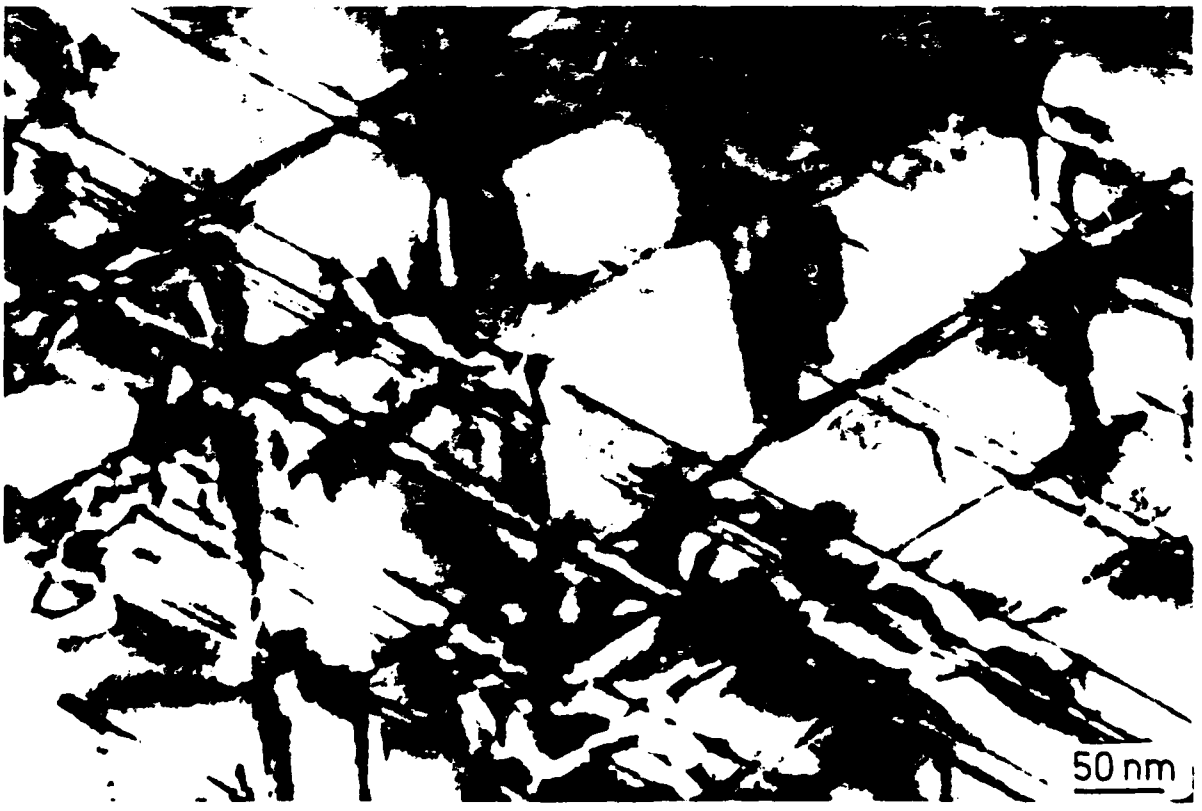

Fig.3

Fig.4a

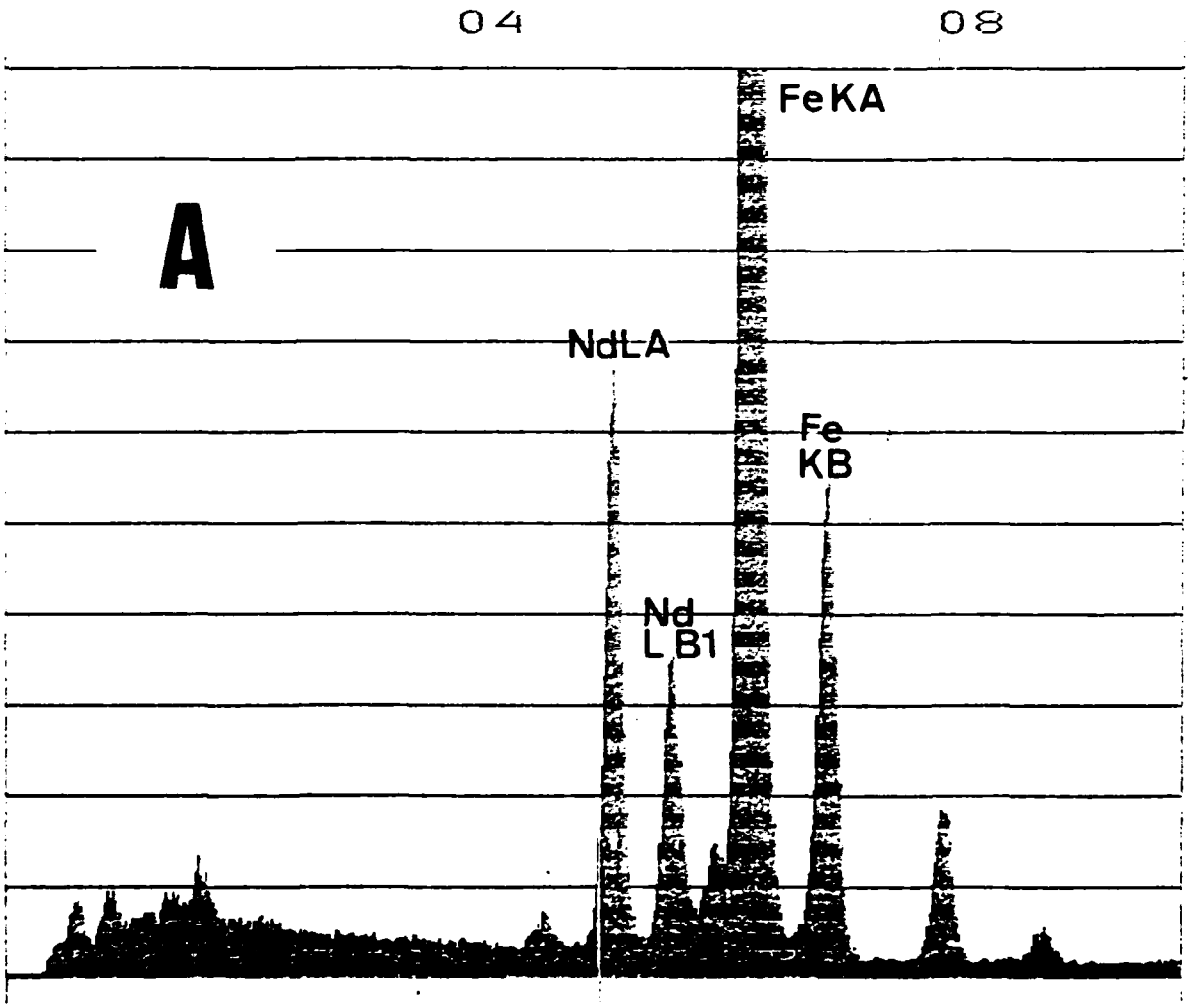

Fig.4b

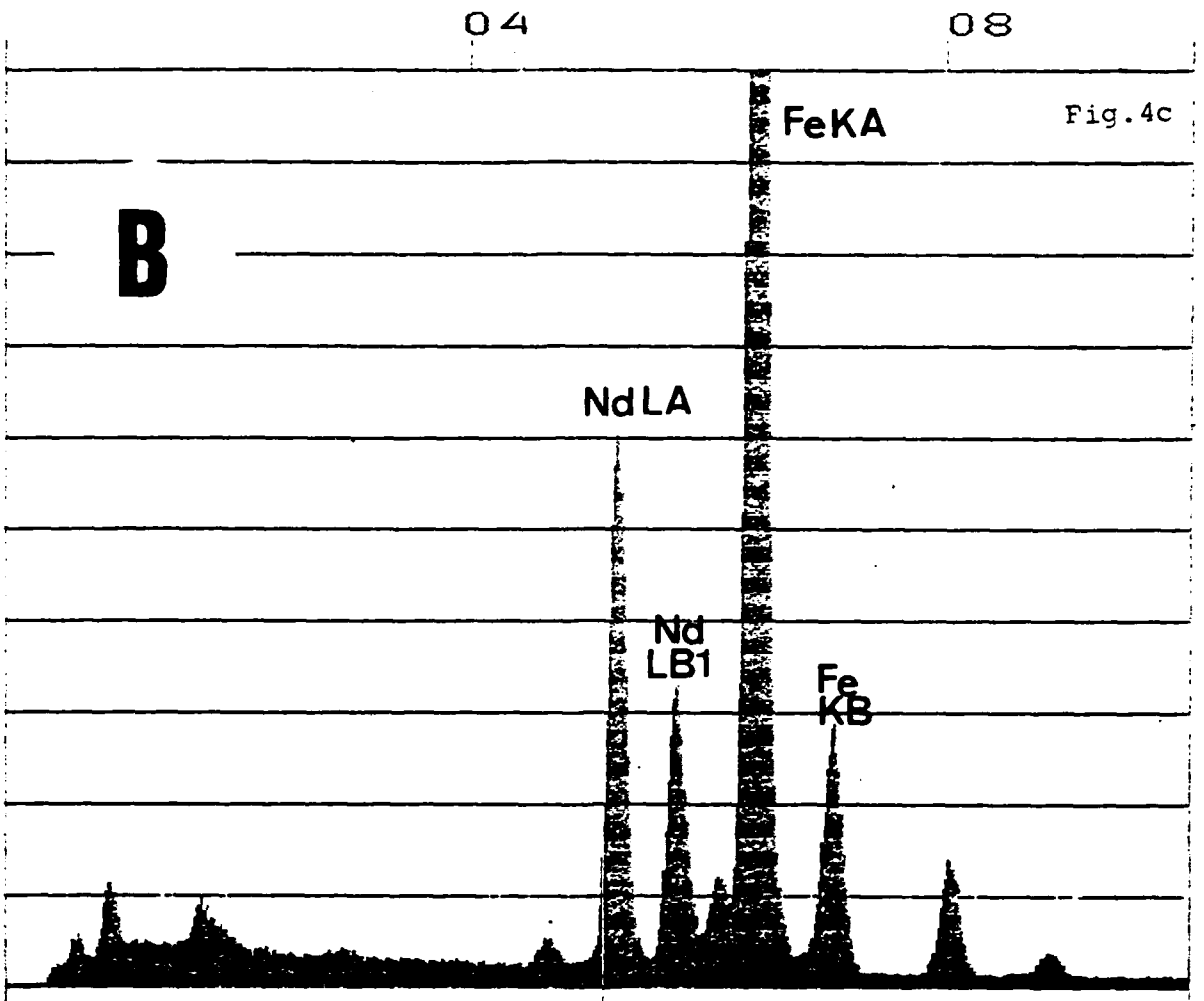

Fig.4c

Fig.4d

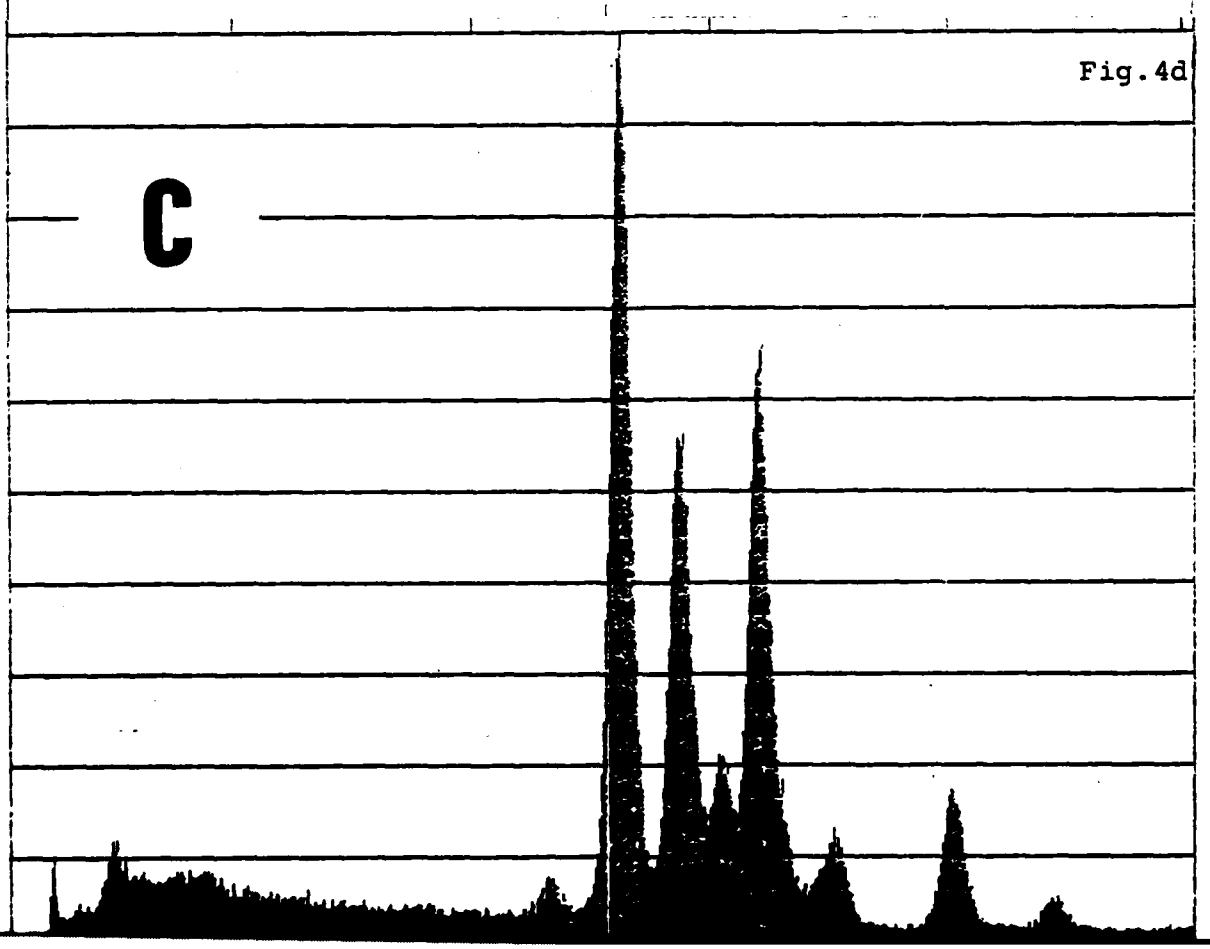

Fig.5a

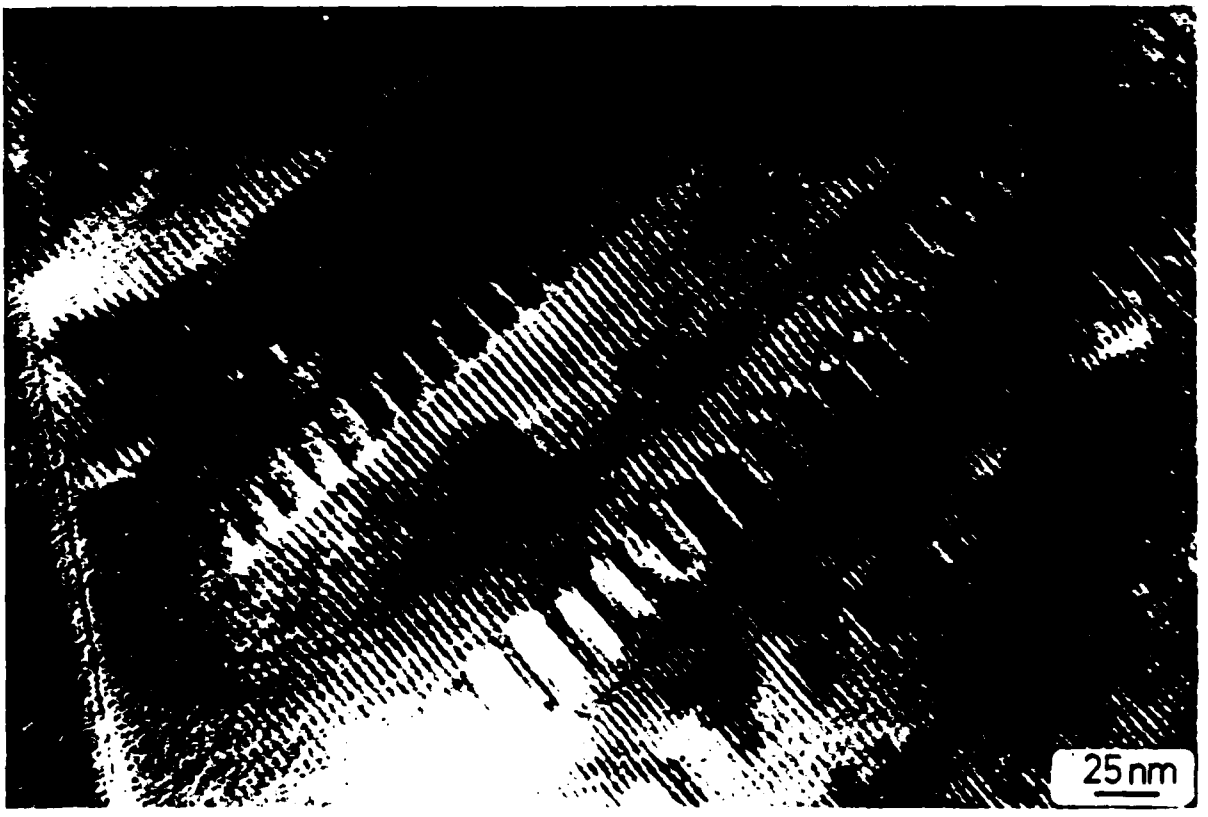

Fig.5b

Fig.6

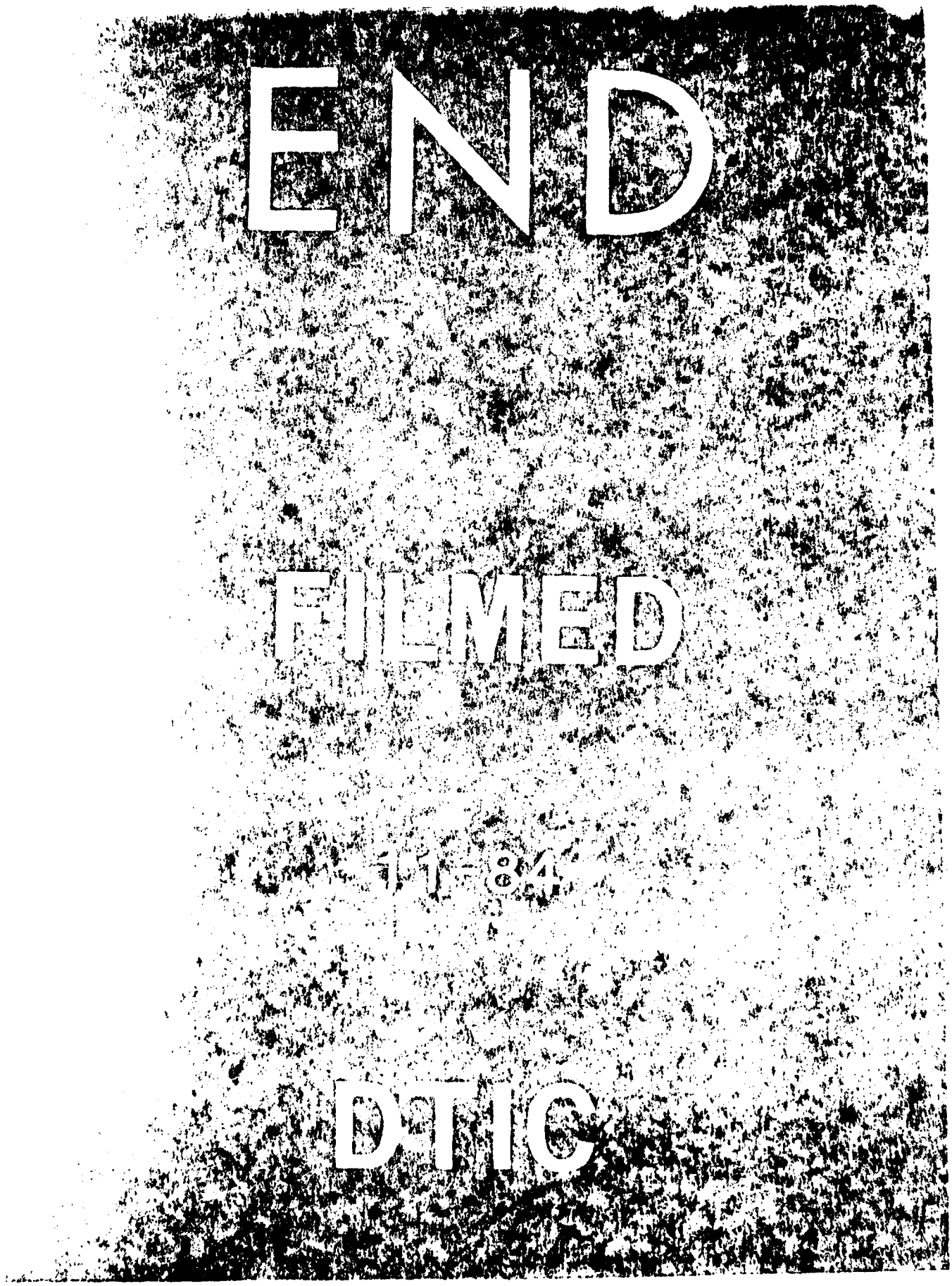
END
FILMED
11-84
DTIC